Deposition angle tunes low-temperature electronic transport in early transition metal thin films

Nicolas Martin [1 *], Hamidreza Gerami [1], Antonio J. Santos [2,3], Francesco M. Morales [2,3], Fabien Amiot [4], Jean-Marc Cote [1], Joseph Gavoille [1], Jean-Baptiste Sanchez [4], Aurélien Besnard [1]

[1] Université Marie et Louis Pasteur, SUPMICROTECH, CNRS, Institut FEMTO-ST, F-25000 Besançon Cedex, France

[2] IMEYMAT: Institute of Research on Electron Microscopy and Materials of the University of Cádiz, E-11510, Puerto Real, Spain

[3] Department of Materials Science and Metallurgic Engineering, and Inorganic Chemistry, Faculty of Sciences, University of Cádiz, E-11510 Puerto Real, Spain

[4] Université Marie et Louis Pasteur, CNRS, Institut FEMTO-ST, F-25000 Besançon Cedex, France

* Corresponding author: nicolas.martin@femto-st.fr

Highlights

- Electron scattering mechanisms are studied through resistivity *vs.* temperature from 7 to 300 K.

- The Bloch-Grüneisen function well describes the electrical properties of hcp metal films.

- Resistivity of bcc metal films saturates at high temperature consistent with the Mott-Ioffe-Regel limit.

- Electron scattering is more complex in Cr films with multiple temperature-dependent effects.

Graphical abstract

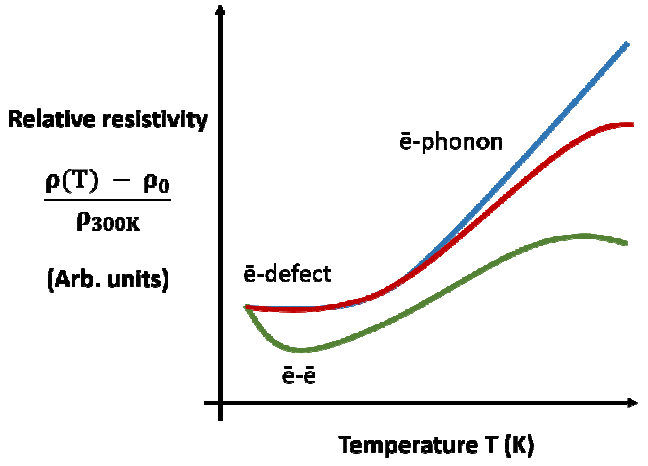

1 Ti, Zr, Hf films

$$\rho(T) = \rho_0 + \rho_{BG}$$

2 V, Nb, Mo, Ta, W films

$$\rho(T) = \rho_0 + \frac{1}{\frac{1}{\rho_{Sat} - \rho_0} + \frac{1}{BT + CT^2}}$$

3 Cr films

For 7 K < T ≤ 150 K

$$\rho(T) = \rho_0 + \frac{\rho_0^{res}}{1 + \left(\frac{T}{\theta^{res}}\right)^2} + D \times \left(\frac{T^5}{\theta^6}\right) \times \int_0^{\frac{\theta}{T}} \frac{x^5}{(e^x - 1)(1 - e^{-x})} dx$$

For 150 K ≤ T ≤ 300 K

$$\rho(T) = \rho_0 + \frac{1}{\frac{1}{\rho_{Sat} - \rho_0} + \frac{1}{BT + CT^2}}$$

Abstract

Nine transition metals, namely, Ti, V, Cr, Zr, Nb, Mo, Hf, Ta, and W, are DC sputter-deposited by oblique angle deposition (OAD). The deposition angle α is gradually changed from 0 to 85° while keeping the films thickness at 400 nm. The electronic transport properties of these metallic nanocolumnar thin films are investigated by means of resistivity *vs*. temperature measurements from 7 to 300 K. Electron scattering phenomena by phonons, defects and electrons strongly depend on the nature of deposited metal, and deposition angle. Temperature-dependent models are applied as a function of the different electron interaction mechanisms. It is shown that the conventional Bloch-Grüneisen theory of bulk metals well explain the electronic transport properties of hcp metals. However, it cannot fit with the various evolutions of resistivity *vs*. temperature measurements of bcc thin films. A saturation effect in resistivity occurs for bcc metals when they are fabricated with the most glancing deposition angles ($\alpha > 70°$). A more complex behavior is also obtained for chromium thin films, which clearly illustrates the significant deviation from the Matthiessen's rule due to the increasing number of growth-induced defects and voids favored by the OAD process.

Keywords: Oblique Angle Deposition, Thin Films, Transition Metals, Resistivity, Temperature, Electron Scattering.

1. Introduction

For the last decades, metallic thin films have received widespread attention since they can be easily used for various applications in microelectronics, corrosion-resistant coatings, optical filters, catalysis among others [1]. Although operating with such films often appears to be non-challenging task and in spite of some remarkable progress in understanding electron scattering phenomena in many monometallic materials, several studies on the electrical conductivity of these films have attracted much attention due to the significant reduction compared to the bulk values and the size effect, especially at the nanometric scale [2, 3]. As a result, understanding the electronic transport properties in monometallic thin films still remains a first ranking scientific motivation, particularly at very low temperatures since electron scattering strongly depends on interactions with impurities, defects, grain boundaries, phonons and so on. Various scattering phenomena predominate depending on temperature. In addition, the dimension of the system (1D for wires, 2D for thin films or 3D for bulk materials) influences the flux of conduction electrons [4]. Thus, electron scattering can be strongly affected in thin films exhibiting different structures at the micro- and nanometric scales and therefore plays a decisive role in the resistivity behavior of nanostructured thin films [5].

Experimentally, the temperature dependence resistivity of thin films is a conventional approach for investigating the electron scattering mechanisms requiring measurements with well-controlled and reduced temperature down to a few K [6]. Theoretically, the magnitude and temperature behavior of the electrical resistivity in metallic thin films are often non-trivial to calculate quantitatively. In the most classical model for the electrical resistivity in metals, the latter is presumed to consist of two terms: The residual resistivity due to electron scattering from random potential (defects, impurities), and the temperature dependent part of resistivity assigned to electron scattering from lattice vibrations of atoms, *i.e.*, phonons [7, 8]. This last contribution is commonly described by the Bloch-Grüneisen equation. According to the Matthiessen's rule, these two contributions are assumed to be independent on each other, and thus the total resistivity is a simple linear combination of these two contributions. For bulk metals and metallic alloys, the Bloch-Grüneisen theory can be successfully applied to many systems. It allows an accurate prediction of resistivity *vs.* temperature evolution from a few K up to

room temperature [9-11]. For thin films, grain boundaries and growth-induced defects become substantial. Electron scattering is favored and discrepancy with the Bloch-Grüneisen theory frequently occurs [12, 13]. As a result, it has been reported for years that significant deviations from the Matthiessen's law exist in many metallic thin films [14-17]. Recently, some authors clearly showed that such deviations can be particularly noticeable in films containing impurities, porous structures, or structural defects [18]. Some mechanisms of electron scattering have been suggested with a temperature dependence such as electron-electron [19], electron-defect [20], or electron-phonon interactions, which are the most reported phenomena [21]. Interference between these mechanisms can also occur over a given range of temperatures (related to the Debye temperature) leading to some inconsistencies with the Bloch-Grüneisen law [22]. In metallic thin films exhibiting a columnar nanostructure, electronic scattering can be modified compared to bulk materials due to size effects, grain boundaries, surface roughness, structural defects, and so on. When the films are prepared by unconventional vacuum processes, especially by oblique angle deposition (OAD), the columnar architecture may become more complex producing unusual metallic behaviors [23]. One can easily figure out that there is a lack of knowledge about electronic transport properties at cryogenic temperatures of OAD metallic thin films since only a few studies have been reported in the literature [24-26].

The motivation of this article lies in understanding the electron scattering mechanisms in monometallic thin films sputter-deposited by oblique angle deposition. Nine transition metals belonging to groups 4, 5 and 6 (also called "early" transition metals): Ti, V, Cr, Zr, Nb, Mo, Hf, Ta, and W, with a thickness of 400 nm, are prepared by DC sputtering using a gradual change of the deposition angle α from 0 to 85°. The electronic transport properties of these nanocolumnar films are investigated by means of resistivity *vs.* temperature measurements from 7 to 300 K. Different temperature-dependent models are applied depending on the electron scattering mechanisms. The conventional Bloch-Grüneisen theory successfully explains the electronic transport properties of metallic thin films adopting the hexagonal-close-packed structure (hcp), whereas a saturation effect of resistivity occurs for body-centered cubic (bcc) metallic thin films especially when they are sputtered

with the highest glancing deposition angles. A more complex behavior is obtained for chromium thin films with an unusual resistivity temperature-dependence and a substantial deviation from the Matthiessen's rule.

2. Material and methods

Thin films were prepared on glass substrates from pure metallic targets (with a purity higher than 99.9 at.% for all metals and a diameter of 51 mm) in a homemade DC magnetron sputtering system. The latter was a 40 L vacuum chamber evacuated with a turbomolecular pump backed by a primary pump. This pumping unit reached a residual pressure lower than 10^{-5} Pa. The distance between the center of the substrate and the target was 65 mm. The target was sputtered in a pure argon atmosphere with a flow rate of 2.6 sccm. For all depositions, a constant pumping speed of 13 L s^{-1} was used producing an argon sputtering pressure of 0.3 Pa. The target current was fixed at 200 mA for all depositions. Glass substrates were grounded during all depositions with no external heating. Before depositing, they were ultrasonically cleaned in acetone and ethanol. The deposition angle α was progressively changed using the following angles: 0, 30, 60, 70, 80 and 85°. The deposition time was adjusted to get the same film thickness (obtained by profilometry) of 400±20 nm for each deposition angle.

DC electrical resistivity measurements were systematically performed from 7 to 300 K for all thin films deposited on glass substrates (5×5 mm^2) using the four-probe van der Pauw method. Such a method, following the NIST procedure (National Institute for Standards and Technology) allows reliable measurements with four gold tips located at the circumference of the sample. A cryostat system from Advanced Research Systems Incorporation (ARS cryocooler series CS-204-AE) was used to cool the sample temperature down to about 7 K in a chamber equipped with a pumping system leading to a vacuum below 10^{-4} Pa. A temperature ramp of 1 K min^{-1} was applied for all resistivity measurements. Relative error on resistivity and temperature values was around 1%.

A homemade software tool was developed for fitting DC electrical resistivity *vs*. temperature with equations describing the different electron scattering mechanisms using the PyCharm Python

Integrated Development Environment (IDE): PyCharm Community Edition 2023.2.1 version. To minimize the relative error between measurements and theory, the Nelder-Mead simplex algorithm was implemented with the number of parameters adapted to the equations describing the electronic transport properties.

3. Results

For the nine transition metals, DC electrical resistivity ρ *vs.* temperature T exhibits a metallic-like behavior for a deposition angle α gradually increasing from 0 to 85°, as typically illustrated for Ti, Zr and Hf films in Fig. 1 (and also shown in Supplementary Materials: cf. Fig. S1 and S2 of section I for the other transition metals). For temperatures higher than a few tens of K, resistivity shows a typical linear evolution with temperature, whereas it becomes constant as the temperature decreases towards 0 K. This ρ *vs.* T linear evolution is commonly encountered in nonmagnetic metallic crystalline compounds. It is mainly assigned to electron-phonon interactions. When the temperature is reduced to a few K, the temperature becomes temperature independent and corresponds to the residual resistivity, namely ρ_0 (Ω m), which is related to electron scattering by defects. As typically reported, and as applied in this study, resistivity measured at 7 K will be assumed as the residual resistivity (*i.e.*, $\rho_0 \approx \rho_{7K}$). For conventional films and for the nine investigated metals, the resistivity of films deposited by the conventional method ($\alpha = 0°$) presents values higher than those of the bulk (about one order of magnitude), as usually observed and in agreement with the Matthiessen's rule [27]. The latter assumes a linear combination of resistivity attributed to two effects: electron-defect and electron-phonon scattering. It also supposes that there are no interactions between these two effects. Due to the polycrystalline structure of sputter-deposited thin films, the electron mean free path is limited by the crystal size, and is systematically lower than that of bulk metals. When the deposition angle increases from 0 to 85° and for all metals, the classical ρ *vs.* T curve is shifted to higher resistivity values, as clearly illustrated for Ti, Zr and Hf metallic films in Fig. 1.

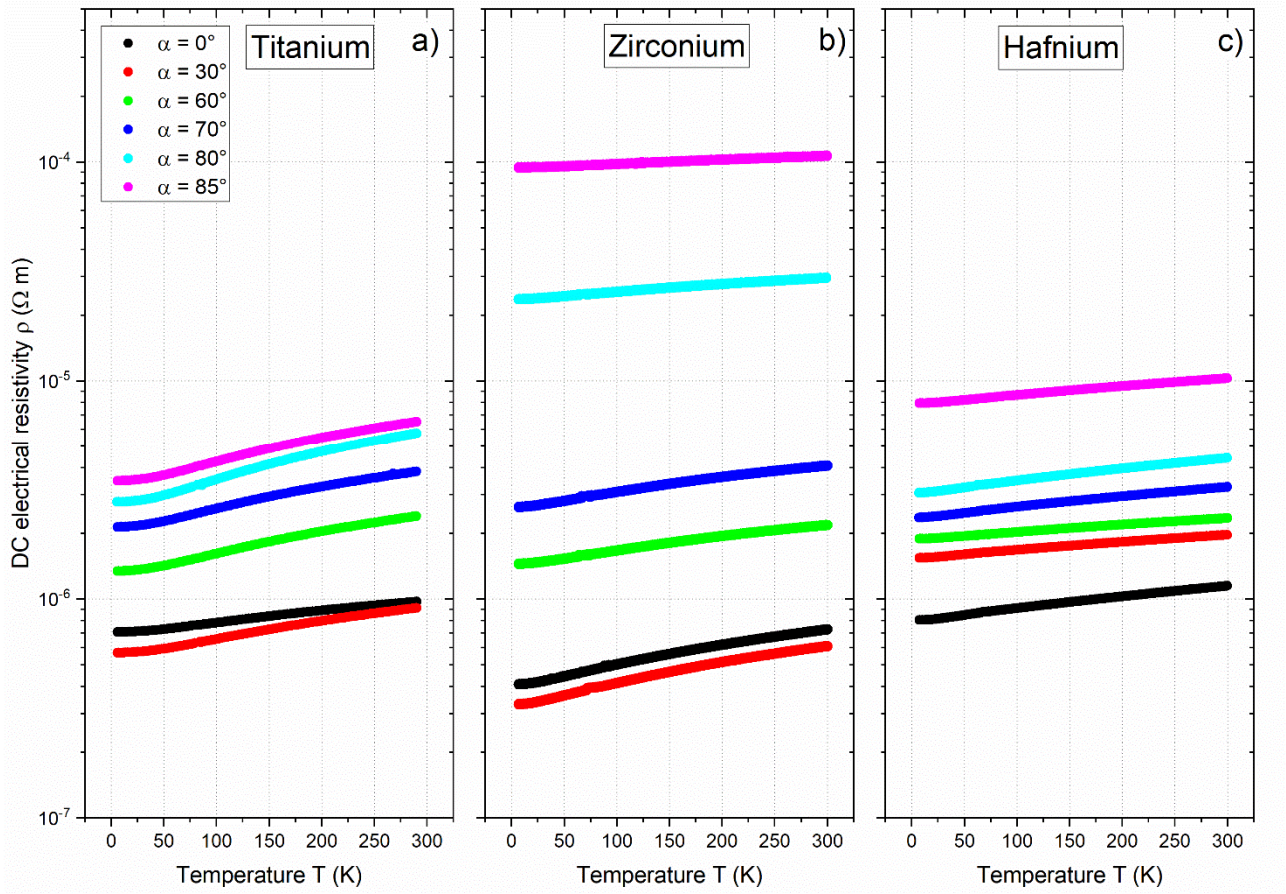

Figure 1: DC electrical resistivity ρ as a function of the temperature T and for different deposition angles α changing from 0° to 85° of: a) Titanium; b) Zirconium and c) Hafnium 400 nm thick films sputter-deposited on glass substrates. A typical metallic-like behavior is measured for these hcp metallic films with a residual resistivity at very low temperature (T less than around 10 K) exhibiting a nearly temperature-independent evolution, whereas a linear temperature-dependence appears when temperature increases and tends to the room temperature.

Films prepared with a deposition angle α = 0 or 30° exhibit very close ρ *vs.* T behaviors, whereas resistivity rises when α is higher than 60°. This deposition angle is often reported as a critical angle required to observe significant modifications of many physical properties in OAD thin films [28]. At this angle, the shadowing effect becomes pronounced, enhancing the porous columnar structure and favoring a high concentration of structural defects. Mean free path of electrons is then reduced due to barrier potential created by voids between columns, and elastic collisions with defects. As a result, the

most resistive metallic films are always produced when the deposition angle tends to the normal deposition, *i.e.*, for $\alpha = 85°$ in our study.

It is also worth noting that for deposition angles varying from 0 to 85°, the jump of resistivity is lower than one order of magnitude for Ti films (ρ is around 10^{-6} Ω m in Fig. 1a), whereas for Zr films the amplitude spans over a bigger range, *i.e.*, from 3×10^{-7} to more than 10^{-4} Ω m, while maintaining the metallic-like behavior as a function of the temperature (Fig. 1b). At first, this increase of resistivity in OAD metallic films as the deposition angle approaches grazing values, can be assigned to a reduction of the electron mean free path. Increasing the α angle leads to more tilted, defined and separated columns. A much more voided and fibrous structure is produced, which favors the electron scattering by surfaces and grain boundaries induced by the enhanced porous structure, the latter being promoted as the deposition angle tends to 90° [29]. It is also worth remarking that because of the significant porosity in OAD metallic films, oxygen may diffuse and produce oxide compounds that certainly contribute to the resistive behavior. However most of the studied films exhibit oxygen concentration around 5 to 10 at.%, and sometimes more for some metallic films (cf. Supplementary Materials) without a clear evolution as a function of the deposition angle. As a result, the large increase of resistivity is mainly attributed to the enhanced electron scattering by grain boundaries, interfaces between columns (voided structure) and structural defects.

All three metals Ti, Zr and Hf adopt the hcp structure. Although the reduction in crystal size (especially when the deposition angle is higher than 60°; cf. Supplementary Materials in [30] for XRD patterns) contributes to the increase of the film resistivity, it does not explain the different amplitudes of resistivity clearly measured for these metals in Fig. 1. For Ti films, the resistivity variation is barely one order of magnitude for a given temperature, whereas Zr films exhibit the biggest jump when α changes from 0 to 85° (*e.g.*, at 300 K more than two orders of magnitude are measured since ρ_{Zr} ($\alpha = 0°$) = 7.37×10^{-7} Ω m and ρ_{Zr} ($\alpha = 85°$) = 1.08×10^{-4} Ω m). Such a strong resistivity variation in Zr films is related to the occurrence of structural defects such as vacancies, dislocations, and interstitials. Former investigations have ever reported that in OAD films the concentration of this kind of defects is favored

as the deposition angle rises [31, 32]. Because of the directional character of the sputtered particles impinging on the growing films, the shadowing phenomenon becomes a predominant parameter producing more voids between columns and thus reducing the film density (cf. [30] and Supplementary Materials for SEM observations). Structural defects such as column biaxial alignment or branching [33], vacancies and interstitials [34] are of crucial importance for the film structure and the resulting electronic transport properties of metallic compounds. Among, Ti, Zr and Hf, the metal that typically retains the highest concentration of structural defects (vacancies, dislocations, or interstitials) under similar fabrication conditions is generally zirconium. The latter tends to retain more defects due to slower self-diffusion rates than Ti and Hf at comparable temperatures [35]. This means that vacancies and interstitials recombine and migrate more slowly, leading to longer persistent defects. On the other hand, Hf is a dense and heavy metal that exhibits a low concentration of defects since they can be easily recombined or trapped in the lattice. As a result, one can expect the most significant variation of resistivity in Zr OAD thin films.

From ρ *vs.* T measurements, the derivative at 100 K, namely $(d\rho/dT)_{100\ K}$, is as simple and noteworthy parameter to characterize the electron-phonon interactions and commonly assumed as a measure of the electron-phonon coupling constant [36]. Similarly, the residual resistivity taken at 7 K, namely ρ_{7K}, is also an interesting data since it is directly related to electron scattering by defects. Both parameters, $(d\rho/dT)_{100\ K}$ and ρ_{7K} have been determined and plotted for all metals sputter-deposited by conventional sputtering ($\alpha = 0°$), with the highest deposition angle ($\alpha = 85°$) and for bulk materials [37] (Fig. 2). As expected, bulk materials exhibit the lowest $(d\rho/dT)_{100\ K}$ and ρ_{7K} values since electron mean free path is supposed to be the longest (a few tens nm in a single crystal), and metals are intended to show the highest purity (lowest concentrations of structural defects). For conventional films ($\alpha = 0°$), slope at 100 K remains nearly the same as the bulk value for all metals. Although the mean free path of electrons is reduced in films due to the decrease in crystal size (typically a few tens nm [30]) compared to single crystal, the strength of the electron-phonon coupling is kept. Such a strength can be affected by the crystal size**,** especially when the latter is reduced to the nanoscale. On the other hand,

residual resistivity is strongly influenced by the deposition angle, as it increases with ρ_{7K} for thin films prepared with $\alpha = 0°$ in-between 10^{-7}-10^{-6} Ω m, whereas it is lower than 10^{-8} Ω m and goes down to a few 10^{-13} Ω m for bulk metals.

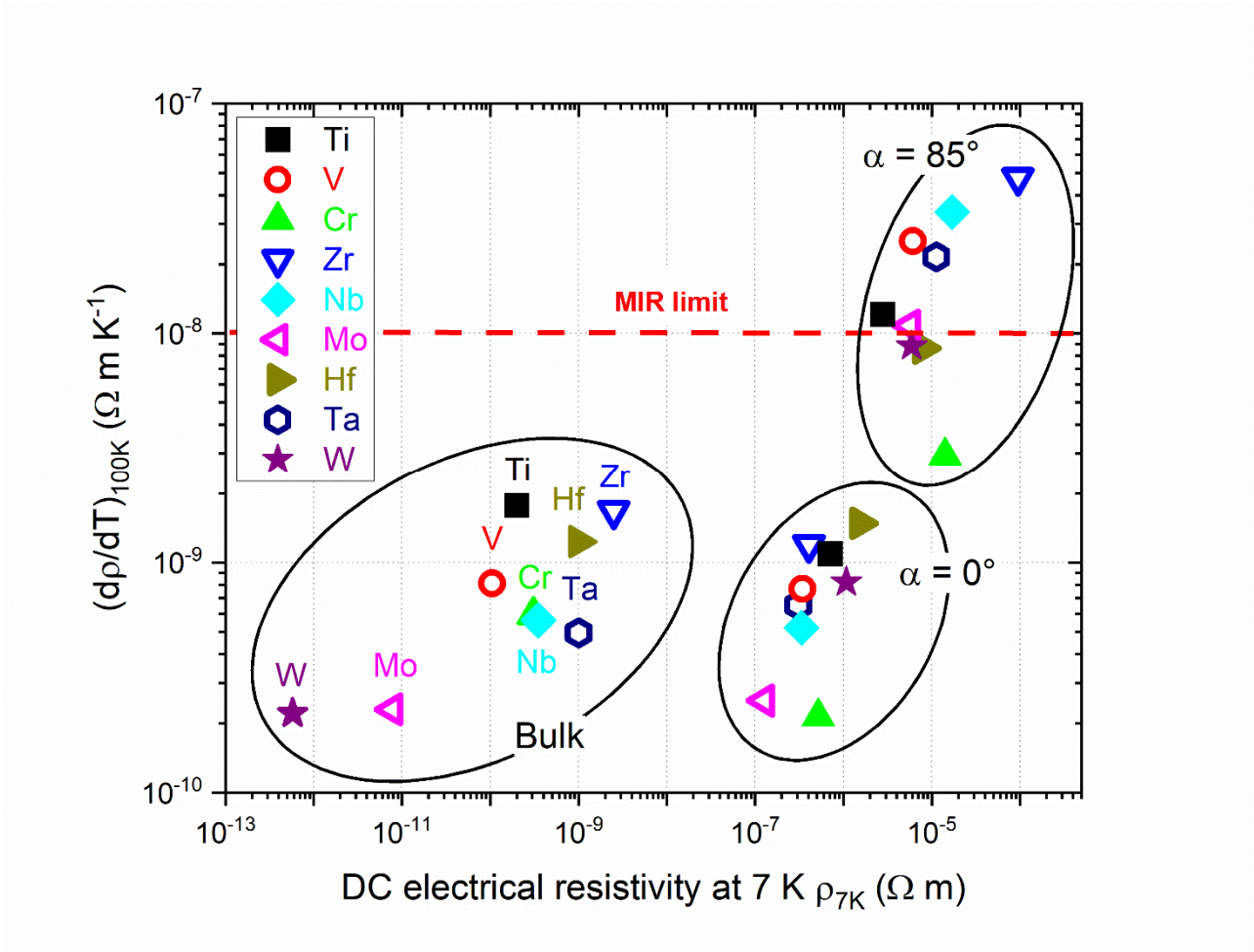

Figure 2: Derivative of resistivity by temperature at 100 K $(d\rho/dT)_{100K}$ vs. DC electrical resistivity at 7 K ρ_{7K} for the three hcp (Ti, Zr, Hf) and the six bcc (V, Cr, Nb, Mo, Ta, W) metallic thin films. Bulk data from [37] can be compared to the film values obtained for conventional sputtering (α = 0°) and the highest deposition angle (α = 85°). The Mott-Ioffe-Regel (MIR) limit is also specified (red dashed line).

Growing defects, impurities as well as the polycrystalline structure commonly produced in conventional thin films disturb the electron mobility in the metal. In addition, because of the sputtering conditions (no external heating during growth and an argon pressure of 0.3 Pa) and the resulting columnar structure systematically obtained for the nine metallic thin films (cf. Supplementary

Materials in [30]), electron scattering by grain and column boundaries contribute to the increase of residual resistivity.

Depositing with an oblique angle and particularly for the most grazing angle $\alpha = 85°$, $(d\rho/dT)_{100K}$ and ρ_{7K} both increase as illustrated in Fig. 2. As previously noted from ρ *vs.* T measurements in Fig. 1, residual resistivity is around 10^{-5} Ω m (or even higher for some metals) since OAD growth favors structural defects (vacancies, interstitials, grain boundaries) of the columnar architecture and voids between tilted columns. It is worth remarking that for these grazing deposition conditions, the Mott-Ioffe-Regel (MIR) limit (close to 10^{-8} Ω m K^{-1} [38]) is reached and even exceeded for most of the studied metals (red dashed line in Fig. 2). This limit corresponds to the maximum resistivity a metal can reach when the electron mean free path is comparable to or smaller than the atomic distance [38]. In other words, it represents the strongest electron scattering rate (the concept of carrier velocity is lost and electron displacement cannot be viewed as propagating freely), which is well emphasized and illustrated by a resistivity at saturation as the temperature rises. Tending to the MIR limit, the electron mean free path reduces and cannot be smaller than the nearest interatomic distance. For the highest deposition angle of 85°, structural defects and porosity between and inside the tilted columns are particularly favored and thus, metallic films prepared with the most grazing angles exceed the MIR limit, behaving as "bad" metals [38] (cf. § 4.2).

The relative resistivity $(\rho - \rho_{7K})/\rho_{300K}$ is also an interesting indicator of the electronic transport properties in metallic thin films, especially when the temperature changes. Fig. 3 shows this evolution for titanium (hcp), vanadium (bcc) and chromium (bcc) thin films sputter-deposited with the two extreme deposition angles $\alpha = 0°$ and 85°. Plotting this relative resistivity *vs.* temperature is relevant for illustrating the different electron scattering interactions, namely the temperature range corresponding to the electron-phonon-defect interference or saturation effect [39]. In addition, normalizing the measured resistivity better shows the role of the deposition angle on the applicability of the Matthiessen's rule since raw data exhibit various amplitudes of resistivity as α changes and according to the nature of the metal (as previously discussed in Fig. 1).

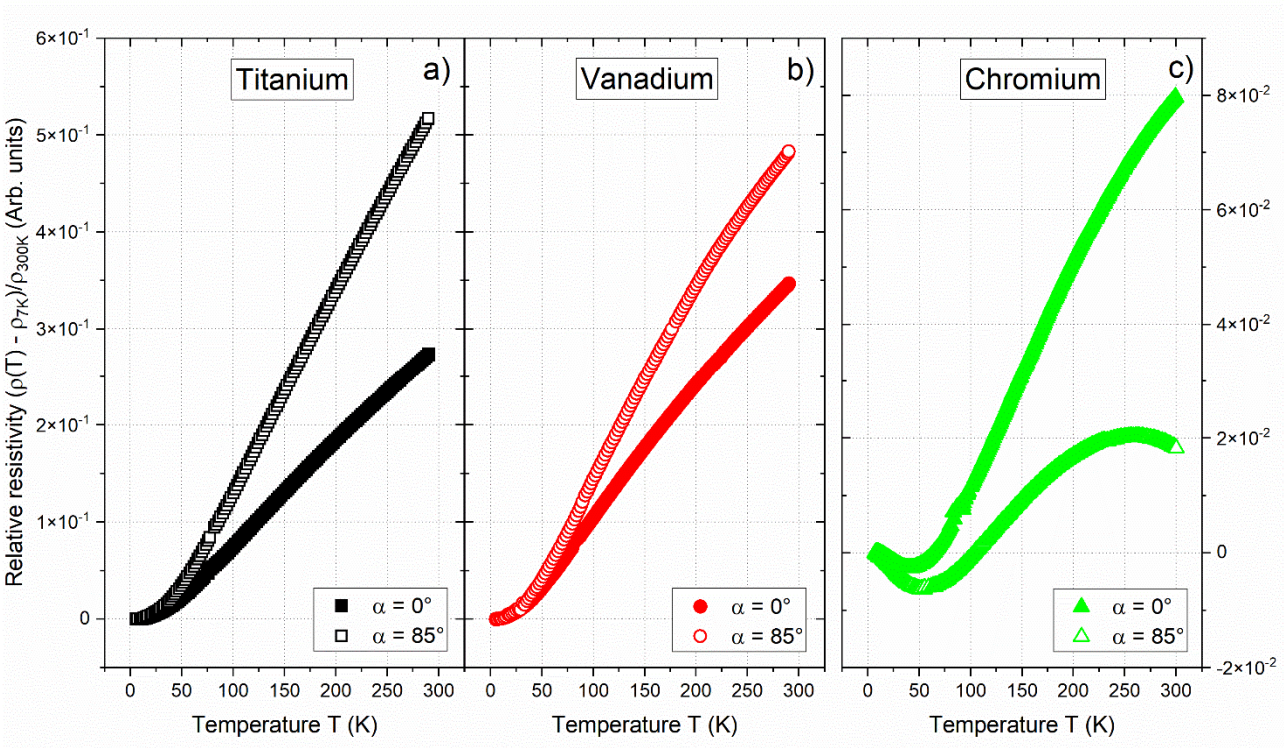

Figure 3: Relative resistivity (ρ - ρ_{7K})/ρ_{300K} vs. temperature T of: a) Titanium (hcp structure); b) Vanadium (bcc structure) and c) Chromium (bcc structure) thin films prepared with two extreme deposition angles α = 0° and 85°. As the temperature rises, a typical linear temperature-dependence is obtained for Ti films, whereas a saturation effect is measured for vanadium films. Chromium films show a minimum value at low temperature and those obtained with a deposition angle α = 85° give rise to an unusual maximum relative resistivity at a temperature T = 262 K.

For titanium films (and similarly for other hcp metals, *i.e.*, Zr and Hf; not shown here but from measurements given in Fig. S1 of Supplementary Materials), the typical metallic-like behavior is clearly obtained. A linear evolution is observed for temperatures down to a few tens of K for the three hcp metals (Fig. 3a). This temperature dependence of the electrical resistivity is mainly attributed to the electron-phonon interaction. When the temperature is lower than about 20 K, the metal resistivity becomes temperature-independent and related to electron scattering by defects (defining the residual resistivity). As the deposition angle increases, all Ti, Zr and Hf films exhibit this linear behavior (with no significant saturation) at high temperature and they become more resistive, which corresponds to a stronger electron-phonon interaction. This increase of relative resistivity with α is also connected to

structural disordering in the films induced by the OAD process. An enhancement of the electron-phonon interaction has been reported in metallic films and depending on the purity and defect concentrations [40]. This is consistent with the increase of a $(d\rho/dT)_{100K}$ and it can be assigned to the softening of phonons [41].

Vanadium films and the four other bcc metals: Nb, Ta, Mo and W all exhibit a similar $(\rho - \rho_{7K})/\rho_{300K}$ *vs.* T behavior. As previously revealed for hcp films, the metallic-like behavior of bcc films is again measured with a constant resistivity for temperatures lower than a couple of tens K, followed by a temperature-dependent resistivity. However, as the temperature rises, resistivity shows an obvious deviation from the linear dependence with a substantial saturation effect of resistivity at high temperature [42] (Fig. 3b). Once more, increasing the deposition angle till the most grazing value leads to more resistive films and emphasizes the saturation. The electron mean free path tends to the nearest-neighbor atomic distance, which correlates with the MIR limit. These results suggest a discrepancy with the Matthiessen's rule and the Bloch-Grüneisen theory is no longer valid (cf. § 4.2).

Regarding the Cr thin films, a more complex evolution of $(\rho - \rho_{7K})/\rho_{300K}$ *vs.* T is recorded as shown in Fig. 3c for the two extreme deposition angles $\alpha = 0°$ and 85°. For temperatures around 50 K and for all deposition angles (cf. Section VII in Supplementary Materials), resistivity exhibits a minimum value that varies with the α angle. This kind of behavior has ever been reported by Boekelheide *et al.* [43] in Cr thin films prepared by magnetron sputtering. The authors showed that this minimum in resistivity at low temperatures is attributed to resonant impurity scattering. They also investigated the effect of the sputtering pressure and post-annealing treatment on the temperature position and minimum value. It was clearly demonstrated that the resistivity minimum is directly related to the number of defects (favored for Cr films grown at high pressure), which are reduced by the annealing. The same argument can be applied for our OAD Cr thin films, *i.e.*, as the deposition angle increases, the most pronounced minimum at $\alpha = 85°$ is similarly due to the increasing concentration of structural defects.

Although relative resistivity shows the saturation phenomenon at high temperature, it does not gradually increase *vs.* α (like in hcp and other bcc metals). An opposite effect is rather measured for α = 85° and even displays a maximum around 2×10^{-2} at T = 262 K. This resistivity maximum is sometimes reported for alloys [44], superconductors [45], or other compounds [46] but remains an unusual feature for simple metallic films. As formerly stated by Krasny *et al.* [47] for amorphous alloys, one may suggest that this emphasis of saturation resistivity leading to a maximum at moderated temperature is due to another scattering of electrons by phonons, *i.e.*, on rotons associated with a minimum in the dispersion curve of longitudinal acoustic excitations (cf. § 4.3).

4. Discussion

4.1. Electron-phonon interactions in hcp metallic films

The temperature-dependent electrical resistivity of the three hcp metallic films (Ti, Zr and Hf) systematically exhibits the typical metallic-like behavior, regardless the deposition angle. It is in agreement with the Matthiessen's rule where resistivity is the sum of two independent electron scattering mechanisms: electron-defect and electron-phonon. As a result, ρ *vs.* T measurements, and specifically the electron-phonon contribution, can be fitted with the Bloch-Grüneisen formula expressed as:

$$\rho(T) = \rho_0 + \rho_{BG} \quad (1)$$

with ρ_0 = residual resistivity that results from structural scatterings due to grain boundaries, impurities, defects, surfaces and so on (Ω m),

$$\rho_{BG} = A \times \left(\frac{T}{\theta}\right)^n \times \int_0^{\frac{T}{\theta}} \frac{x^n}{(e^x-1)(1-e^{-x})} dx \quad (2)$$

and ρ_{BG} is the temperature dependent electrical resistivity phonon scattering (Ω m)

where A = electron-phonon coupling constant (Ω m),

T = temperature (K),

θ = Debye temperature (K),

n = constant taking the values of 2 (electron-electron scattering), 3 (electron-magnon scattering) or 5 (electron-phonon scattering) depending on the nature of electron interactions. In this study, Ti, Zr and Hf are nonmagnetic metals and the dominant charge carrier interaction mechanism involves phonons, so n = 5 has been chosen for the fitting procedure. About residual resistivity and for each sample, the experimental value measured at 7 K has been used as a fixed fitting parameter.

In order to investigate the influence of the deposition angle on electron transport properties in OAD hcp films, the amplitude and temperature behavior of the electrical resistivity were calculated assuming equations (1) and (2) and implementing the fitting procedure using a home-made Python program (cf. Section II of Supplementary Materials). The electron-phonon coupling constant A, as well as the Debye temperature θ, were taken as adjustable coefficients for fitting over the whole temperature range 7-300 K (measured and fitted ρ *vs.* T, along with the corresponding relative error, are shown in Fig. S4, Section III of Supplementary Materials for all hcp films prepared with different deposition angles). Fig. 4 shows fitting results of θ and A *vs.* α for the three hcp metallic films. For all films, Debye temperatures deduced from fitting are systematically lower than the bulk values with θ_{Ti} = 420 K, θ_{Zr} = 291 K and θ_{Hf} = 252 K [37]. These reduced values obtained for films have previously been mentioned for other metallic compounds [48]. Although ρ *vs.* T measurements often give rise to an underestimation of the Debye temperature compared to the heat capacity approach [49], or from elastic constants of the material [50], the effect of the polycrystalline structure inherent to thin films also affects θ, as pointed out by several studies focused on monovalent metallic films [51-53].

Very recently, we also showed that the same deviation to the bulk occurs for OAD Au thin films [54]. These discrepancies systematically recorded for the Debye temperature between bulk and films can be expected assuming that θ is related to the atomic density and sound velocity of the material [55]. Although the sputtering process leads to a quite dense microstructure of thin films, it is well-known that physical and chemical characteristics of films are systematically lower than those of the bulk. Growing defects, impurities and grain boundaries disturb the long-range order and thus influence the film properties. In addition, among the few studies focused on acoustic wave propagation in OAD metallic films, the sound velocity is strongly reduced (divided by 2 or even more compared to the bulk)

due to the porous architecture favored as the deposition angle rises [56, 57]. As a result, a low atomic density as well as a reduced sound velocity both contribute to the lowered Debye temperature obtained for Ti, Zr and Hf OAD thin films.

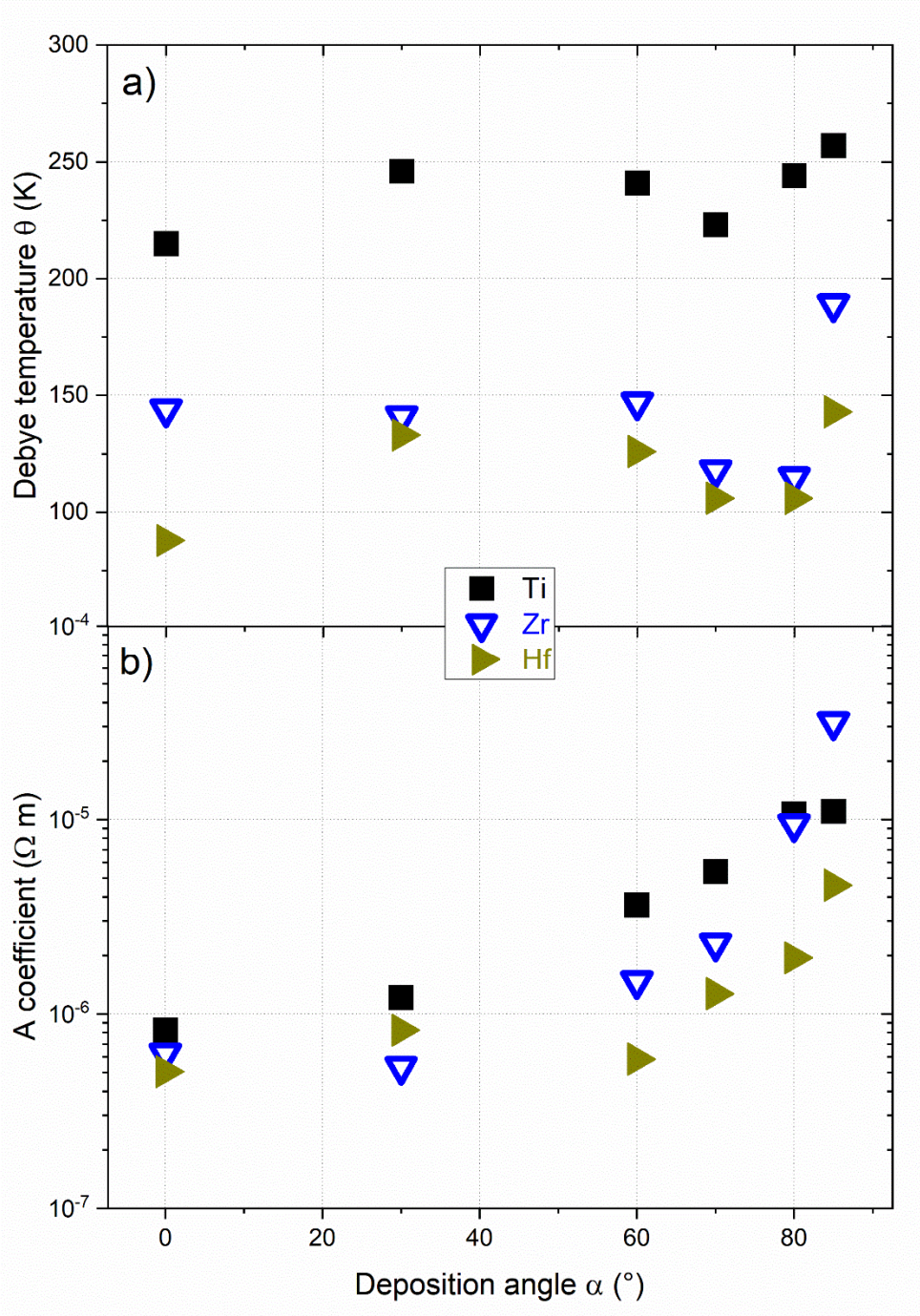

Figure 4: Fitted parameters, namely a) Debye temperature θ and b) A coefficient, determined from the Bloch-Grüneisen law (Eq. (1) and (2)) as a function of the deposited angle α for the three-hcp metallic thin films: Ti, Zr and Hf.

It is also worth noting how the deposition angle influences A and θ as illustrated in Fig. 4. For α angle between 0 and 60°, the Debye temperature exhibits no clear trend, whereas the highest deposition angles (α > 70°) produce a significant increase of θ for the three hcp metals. Regardless of the nature of the deposited OAD thin films (metals, ceramics or semi-conductors), a gradual change of the deposition angle in the 0-50° range does not create the most substantial evolution of many physical properties. For these low angles, shadowing effect does not act as the key parameter of the growing process and despite the formation of a tilted columnar structure, film behaviors are slightly modified as α increases. For the most grazing deposition angles, especially when α overpasses 60° (namely, glancing angle deposition conditions), shadowing effect becomes predominant leading to an increasing number of structural defects, a higher voided structure and consequently, many characteristics of the films change markedly. As a result, one should expect a reduced Debye temperature as the deposition angle tends to grazing values since disorder and defects weaken sound velocity and elastic modulus. From results in Fig. 4a, no clear trend can be seen although the fitted Debye temperatures obtained for the three hcp metallic films exhibit the highest θ values when α reaches 85°.

On the other hand, the A coefficient rises a little as the deposition angle changes from 0 to 60°. A further increase of α up to 85° produces higher A values (around one order of magnitude), and exceeds 10^{-5} Ω m for Ti and Zr films. Based on Yeh *et al.* investigations [58], this A coefficient is directly connected to the electron-phonon interaction, namely the electron-phonon coupling constant. Such a constant represents the softening effect of phonons. Increasing A coefficient with deposition angle means that the electron-phonon scattering rate (depending on the longitudinal-to-transverse phonons ratio) decreases, and so electron scattering is dominated by interactions with longitudinal rather than transverse phonons.

4.2. Saturation of resistivity in bcc metallic films

The temperature-dependent resistivity of metallic thin films may exhibit anomalous behaviors, *i.e.*, saturation phenomenon when the resistivity becomes large enough and as the temperature rises [42]. This was formerly reported for A15 (intermetallic metastable phase) thin films and mainly

attributed to the electron mean free path, which tends to be nearly as small as the lattice constant of the material [59]. The thermal disorder induced by the high temperature lattice vibrations is not the only parameter leading to the saturation resistivity. Some static disorders induced by radiation damage, ion bombardment or growing defects may also generate this saturation effect. As a result, the film resistivity rises with a less than linear temperature dependence and the Bloch-Grüneisen law becomes inappropriate. While hcp metallic films exhibit classical ρ *vs.* T behaviors (*i.e.*, the typical metallic-like behavior whatever the deposition angle), it looks very different for the six bcc films, as illustrated in Fig. 3b and 3c for vanadium and chromium films, respectively (ρ *vs.* T of the other metals can be seen in Fig. S1 and S2, Section I of Supplementary Materials; Cr thin films exhibit more complex characteristics and will be discussed in § 4.3). On the other hand, resistivities of V, Nb, Ta, Mo and W thin films all increase with the deposition angle and their temperature dependence deviates significantly from linearity. In many metallic and alloyed materials, the ρ *vs.* T evolution has been described by Wiesmann *et al.* [60] as a "shunt resistor model" based on a simple-parallel resistor formula:

$$\frac{1}{\rho(T)} = \frac{1}{\rho_{ideal}(T)} + \frac{1}{\rho_{Sat}} \quad (3)$$

where $\rho_{ideal}(T)$ is the ideal resistivity (Ω m) given by the sum of residual resistivity, namely ρ_0, and the resistivity due to electron-phonon interactions, *i.e.*, ρ_{BG}. However, some studies reported that equation (3) is not valid for some transition metals and alloys [61, 62]. Hussey *et al.* [63], and more recently Sundqvist and Tolpygo [64, 65] suggested an approximation of the electron-phonon scattering term giving rise to:

$$\rho_{ideal}(T) = \rho_0 + BT + CT^p \quad (4)$$

with B (Ω m K^{-1}) and C (Ω m K^{-p}) being fitting parameters, and p = 2, 3 or 4 depending on the agreement of the fitting with the data. The same authors also proposed a modified expression of the saturation term based on more realistic values for the fitted parameters, thus obtaining the following equation:

$$\rho(T) = \rho_0 + \frac{1}{\frac{1}{\rho_{ideal}} + \frac{1}{\rho_{par}}} \quad (5)$$

where ρ_{par} (Ω m) is defined from the difference between saturation and residual resistivities: $\rho_{sat} - \rho_0$.

From ρ *vs.* T measurements of V, Nb, Ta, Mo and W OAD thin films and for all deposition angles, the best fits were obtained assuming equation (5) (cf. sections IV and V of Supplementary Materials) with p = 2 and neglecting ρ_0 compared to BT and CT^2 values that produced the following equation:

$$\rho(T) = \rho_0 + \frac{1}{\frac{1}{\rho_{Sat} - \rho_0} + \frac{1}{BT + CT^2}} \quad (6)$$

Therefore, four fitting parameters: ρ_0, ρ_{Sat}, B and C coefficients were determined and optimized by means of a home-made Python program in the entire temperature range 7–300 K (cf. Section IV of Supplementary Materials). As a key parameter, the saturation resistivity ρ_{Sat} is at first plotted as a function of the deposition angle α, and for the six bcc metallic thin films (Fig. 5). All films exhibit the same ρ_{Sat} *vs.* α evolution, *i.e.*, a more or less constant saturation resistivity until α = 60°, followed by an abrupt increase as the deposition angle tends to the grazing angle of 85°. The range of angles around 60° is again a critical value of the OAD process from which many physical properties of the films sharply vary [28]. Since the resistivity at saturation mainly depends on the electron density ($\rho_{Sat} \propto n^{-2/3}$ [64]), and assuming that an increase of the deposition angle develops a voided structure, and a higher number of growing defects as wells as interfaces, the electron recombination is favored. This becomes particularly marked for glancing angles (*i.e.*, α > 70°). The shadowing length exceeds the surface diffusion length of the sputtered atoms impinging on the column apex. The ballistic shadowing effect becomes the key parameter of the film growth that directly impacts the film microstructure and thus the physical properties.

It is interesting to note that the increase of resistivity saturation with the deposition angle is less marked for W, Ta or Cr OAD thin films (barely one order of magnitude between ρ_{sat} obtained at α = 0° and 85°). For these three metals, the lowest variation of ρ_{sat} *vs.* α can be connected to their propensity to develop other phases, especially the non-equilibrium A15 phase. It was previously reported that some bcc transition metals (especially W, Ta and Cr) easily produce this particular A15 metastable phase (A_3B structure) during the film growth when impurity level (oxygen, carbon …) is high enough in vacuum processes [66]. This also occurs in OAD thin films due to their voided structure enhanced

at grazing deposition angles [67]. Investigations focused on electronic transport properties of these bcc metals prone to the A15 phase formation showed a high electrical resistivity when bcc + A15 metastable phases both coexist, which correlates with a high resistivity at saturation for these three metallic thin films, even for the lowest deposition angles.

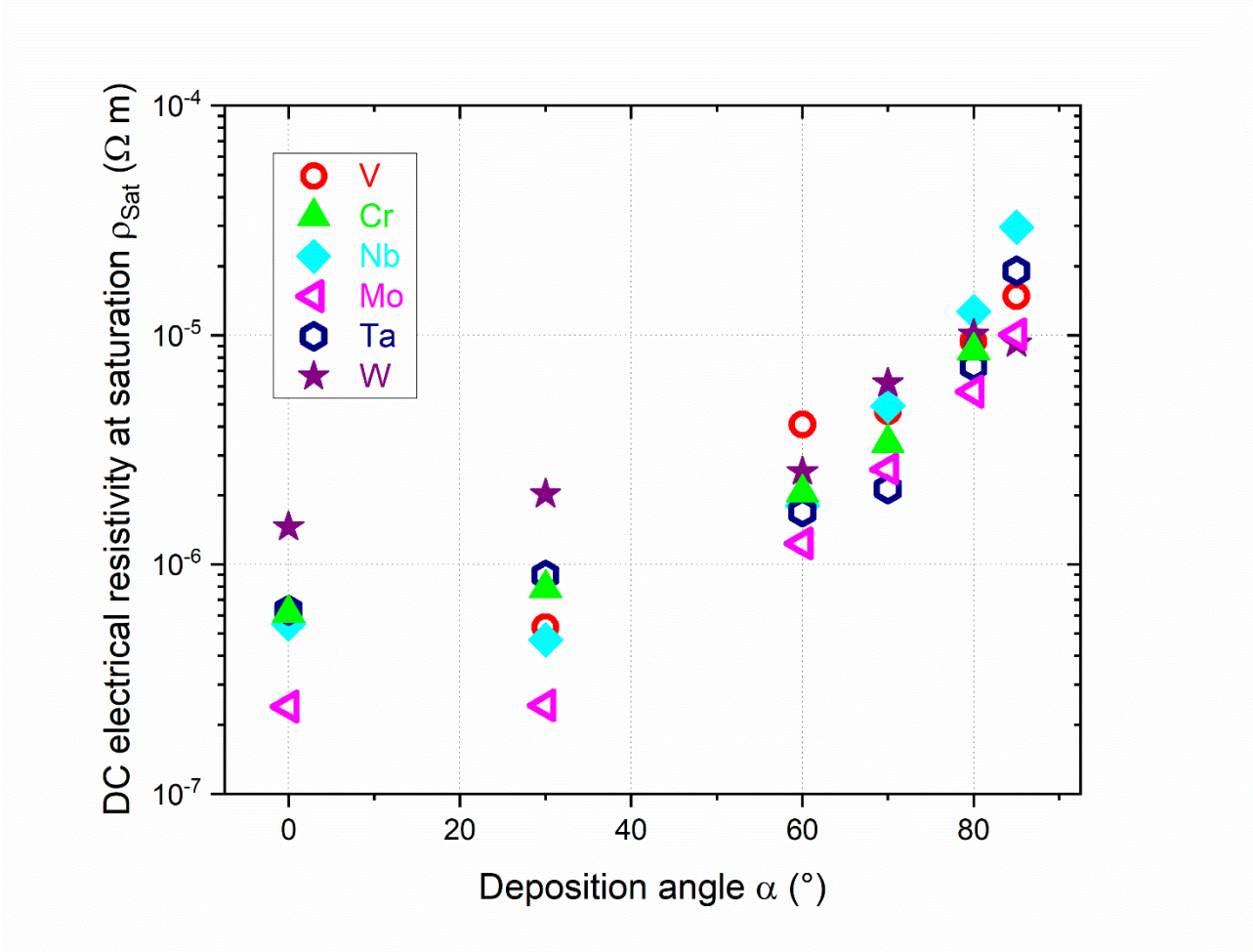

Figure 5: Resistivity saturation ρ_{Sat} as a function of the deposition angle α of the six bcc metallic thin films: V, Cr, Nb, Mo, Ta and W. The resistivity at saturation ρ_{Sat} is determined from fitting ρ vs. T experimental data with equation (6) based on the parallel resistor formalism [60].

So, when the deposition angle changes from 60° to 85° and for all metallic thin films, the resistivity saturation tends to be between 8.56×10^{-6} and 2.95×10^{-5} Ω m (Fig. 5). This also correlates with the MIR limit previously discussed from ρ *vs.* T measurements in Fig. 1. This upper bound of resistivity ρ_{MIR} can be roughly estimated from the Drude model assuming the electron density of the bulk metal, as described in [45]:

$$\rho_{MIR} = \frac{3\,\pi^2\,\hbar}{q^2\,k_f} = \frac{h}{2\,q^2}\left(\frac{9\,\pi\,M}{N_A\,d}\right)^{1/3} \quad (7)$$

where $k_f = (3\pi^2 n)^{1/3}$, n is the effective carrier density (m^{-3}), M the atomic mass (kg mol^{-1}), and d the density (kg m^{-3}) ($\hbar$, h, q and N_A are universal constants). For the six studied metals, ρ_{MIR} ranges from 9.02×10^{-6} (Cr) to 1.03×10^{-5} Ω m (Nb or Ta), which is in the same order of magnitude of the resistivities at saturation obtained for α = 85°.

Based on fitting results and assuming equation (5), residual resistivity and saturation resistivity have been determined for the six bcc metals. Plotting ρ_{sat} *vs.* $\rho_0 \approx \rho_{7K}$ allows an interesting comparison since there are two important but distinct characteristics of electronic transport properties in metals at low and high temperature (Fig. 6). Both resistivities exhibit the same order of magnitude, regardless of the deposition angle. This proves again that there is a breakdown of the Matthiessen's rule of bcc OAD metallic thin films, especially when the deposition angle rises. This is consistent with previous results demonstrating a high number of structural disorders and defects in the columnar structure, as well as a short mean free path of carriers (*i.e.*, free electrons) when α tends to grazing values. As a result, and for the six bcc metallic thin films, residual and saturation resistivities similarly increase with deposition angle. Since imperfections in the metal's structure such as structural defects, impurities, grain boundaries, and so on, contribute to the residual resistivity and knowing that high deposition angles involved in the OAD process favor a voided architecture with an increased number of growing defects, the highest residual resistivities can be expected as the deposition angle tends to be grazing, whatever the metal.

About the resistivity at saturation, we can argue that saturation is not caused by the thermal disorder produced by the high temperature lattice vibrations, but rather to static disorder typically favored by the increase of α. The electron-phonon scattering becomes less significant due to the voided structure and defects. These metallic bcc OAD thin films can be considered as "bad metals", as previously suggested for single metals, alloys and superconductors [38, 59]. In addition, these six studied transition metal thin films are likely to form A15-compounds particularly when the deposition angle rises (cf. Supplementary Materials from [30]). Because of the oxygen stabilizes the A15

metastable phase and assuming the increasing porous structure in OAD thin films, the A15 occurrence may also contribute to the resistivity saturation.

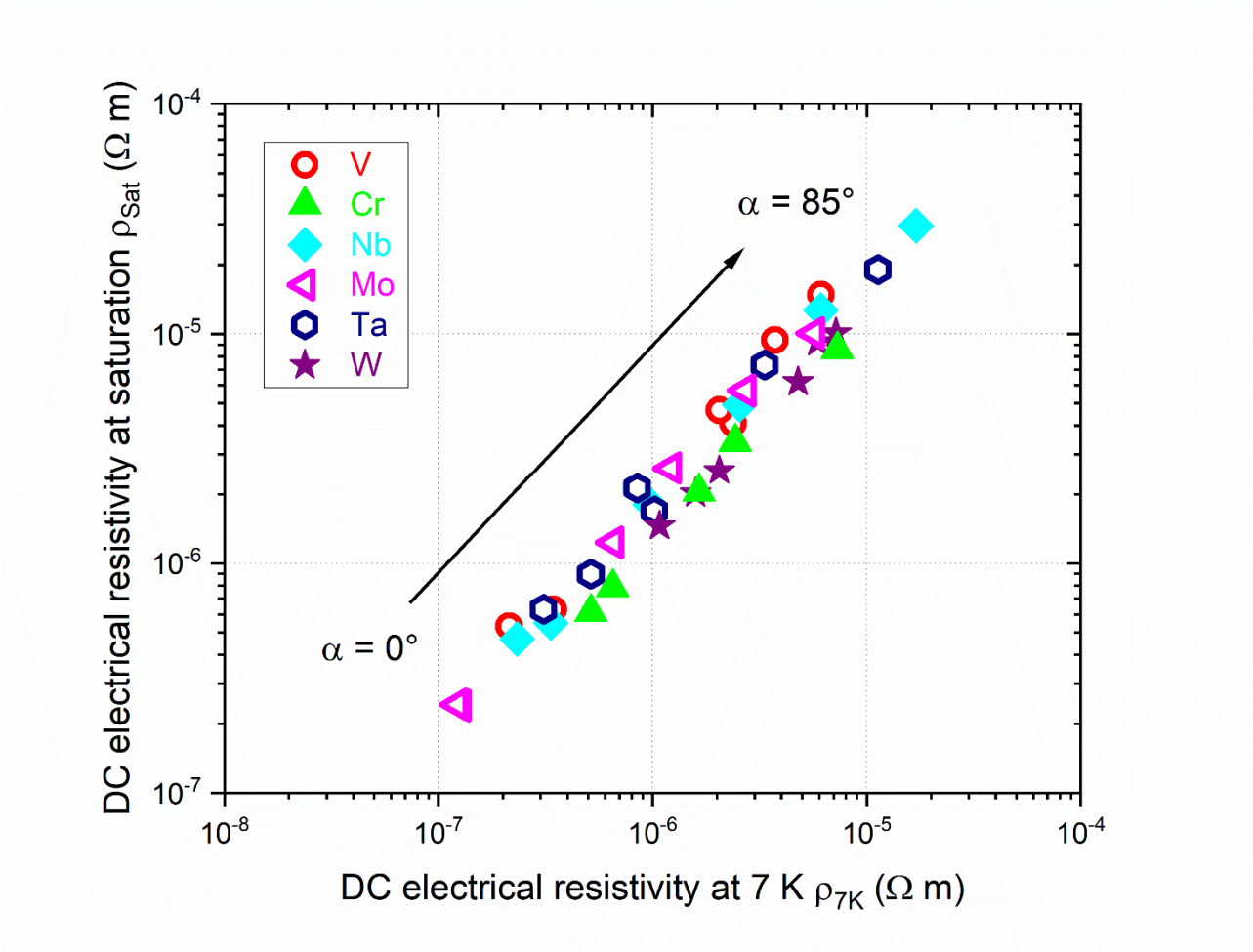

Figure 6: Resistivity saturation ρ_{Sat} as a function of the residual resistivity ρ_0 taken at 7K ρ_{7K} (Log scales) of the six bcc metallic thin films: V, Cr, Nb, Mo, Ta and W. Both resistivities similarly increase (more than two orders of magnitude) when the deposition angle α changes from 0° to 85°. ρ_{7K} measured at 7 K is nearly the same as ρ_0 obtained from fitting ρ vs. T assuming Eq. (5) (cf. Supplementary Materials). ρ_{Sat} is also determined from the same fitting procedure.

Finally, it is interesting to remark that Guo *et al.* [38] reported a similar ρ_{Sat} *vs.* ρ_0 evolution, *i.e.*, a simultaneous increase of both resistivities depending on the nature of the metal, and type of compound (superconductors, conductive oxides, metallic alloys). They relevantly suggested a classification of the metals, *i.e.*, from normal metals for the lowest residual and saturation resistivities

to bad metals when the scattering of electrons by defects or impurities is emphasized, corresponding to the highest residual and saturation resistivities. For these six bcc OAD thin films, an increase of the deposition angle clearly leads to enhanced residual and saturation resistivities with a linear Log-Log evolution. Such evolution illustrates again the growing number of defects in OAD metallic thin films as α tends to the grazing values.

Similarly, B and C coefficients defined from equation (6) can be obtained from the fitting procedure described in sections IV and V of Supplementary Materials. Each coefficient can be plotted *vs.* resistivity at 300 K ρ_{300K} for the six bcc OAD thin films and for an increasing deposition angle (Fig. 7. They both increase as α changes from 0° to 85° with B coefficients that are systematically around two orders of magnitude higher than C coefficients for the same ρ_{300K}. From the expression of ρ_{ideal} in equation (6), this means that resistivity is dominated by a strong linear component at low temperature. According to Guo *et al.* [38], the C coefficient, it is related to the electron-electron scattering phenomenon and encompasses the non-linear character of the scattering rate. On the other hand, the B coefficient is connected to the scattering time of free electrons, *i.e.*, the shortest possible time between electron scattering events limited by the temperature (namely, the Planckian dissipation limit). In other words, increasing this B coefficient correlates with a reduced scattering time (ρ_{sat} contribution is emphasized), which agrees again with a more marked scattering of carriers by defects, impurities and structural disorders in OAD thin films. In addition, the B coefficient tends to saturate to the maximum value of 10^{-8} Ω m K^{-1} for the highest deposition angles, which corresponds to the MIR limit previously discussed for films prepared with grazing deposition conditions (Fig. 2).

However, and for Mo films, although B coefficient evolution is rather spread as α rises, it is not so affected by the deposition angle, whereas C coefficient increases, and even exceeds B. This implies that the saturation effect in Mo films occurs at higher temperature compared to other metals. This behavior can be assigned to the low m*/n ratio (where m* is the effective mass of electrons and n the density of free electrons), which influences electron scattering and transport properties [38]. This low

ratio delays the onset of electron-phonon scattering and thus the resistivity saturation is shifted to higher temperatures.

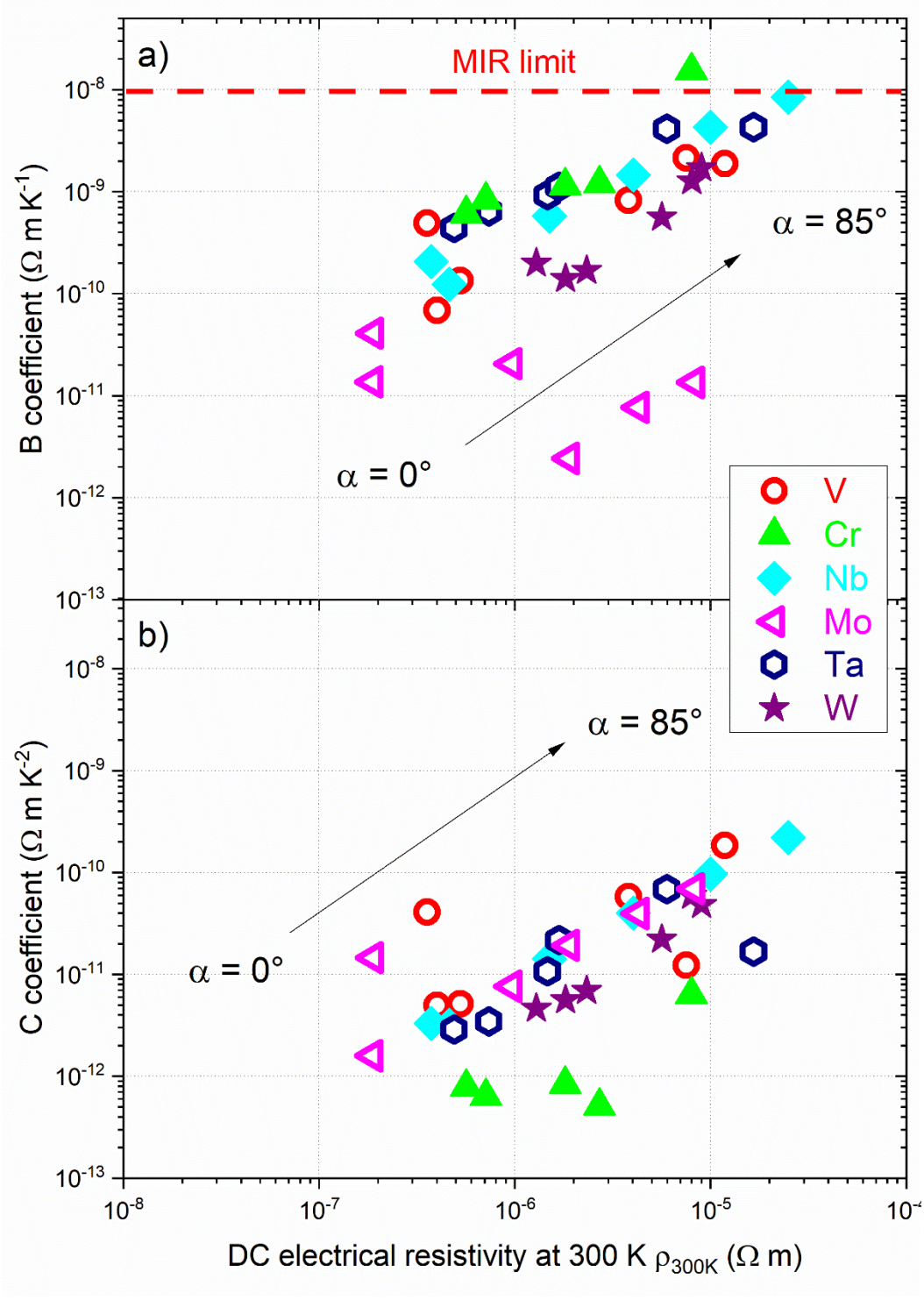

Figure 7: Evolution of a) B and b) C coefficients vs. DC electrical resistivity at room temperature ρ_{300K} for the six bcc metallic thin films: V, Cr, Nb, Mo, Ta and W. Both coefficients are determined from the fit of ρ vs. T data assuming Eq. (6). The Mott-Ioffe-Regel (MIR) limit is indicated with the red dashed line ($B_{MIT} = 10^{-8}$ Ω m K^{-1}). The effect of the deposition angle α is also shown.

A classification of metallic compounds based on ρ *vs.* T measurements can be suitably performed considering the relative importance of B and C coefficients (the magnitude of B/C ratio represents the temperature at which the linear and quadratic terms in Eq. (6) become equal) and the residual resistivity [38, 68]. These two parameters, namely B/C and ρ_0, provide a simple and consistent classification of metallic transport behaviors as shown in Fig. 8 for the six bcc OAD thin films (residual resistivity is taken at 7 K, *i.e.*, $\rho_0 \approx \rho_{7K}$). Compared to bulk values (ρ_0 in-between 10^{-11}-10^{-9} Ω m), residual resistivities of conventional metallic thin films ($\alpha = 0°$) are systematically higher leading to their ranking at least one order of magnitude above the limit of the normal metals in the ρ_{7K} *vs.* B/C diagram (*i.e.*, $\rho_{7K} > 10^{-7}$ Ω m). This high residual resistivity is often reported in sputter-deposited single metallic coatings although the very low vacuum reached or specific operating conditions set in the deposition chambers [69]. Grain boundaries, growing defects and impurities cannot be completely prevented in such films giving rise to a relatively high residual resistivity, especially for W films where ρ_{7K} is around 10^{-6} Ω m. Its reactivity towards oxygen and difficulty in obtaining very pure and defect-free crystals in sputtered W thin films (easily occurrence of the A15 phase) favor electron-defect scattering.

It is also worth remarking how B/C and ρ_0 both vary *vs.* α, but above all, depending on the nature of the metal. As expected, increasing α from 0° to 85° produces a more voided material and a rising number of structural defects. The resistivity development is attributed to the enhancement of the electron scattering by surfaces and grain boundaries induced by a much more porous film's architecture. The latter is promoted as α tends to 90°. This result (certainly extended to other metals) is clearly illustrated in Fig. 8 since for the six bcc metals, residual resistivity systematically increases of more than one order of magnitude, reaching and even exceeding 10^{-5} Ω m for metals like Nb and Ta.

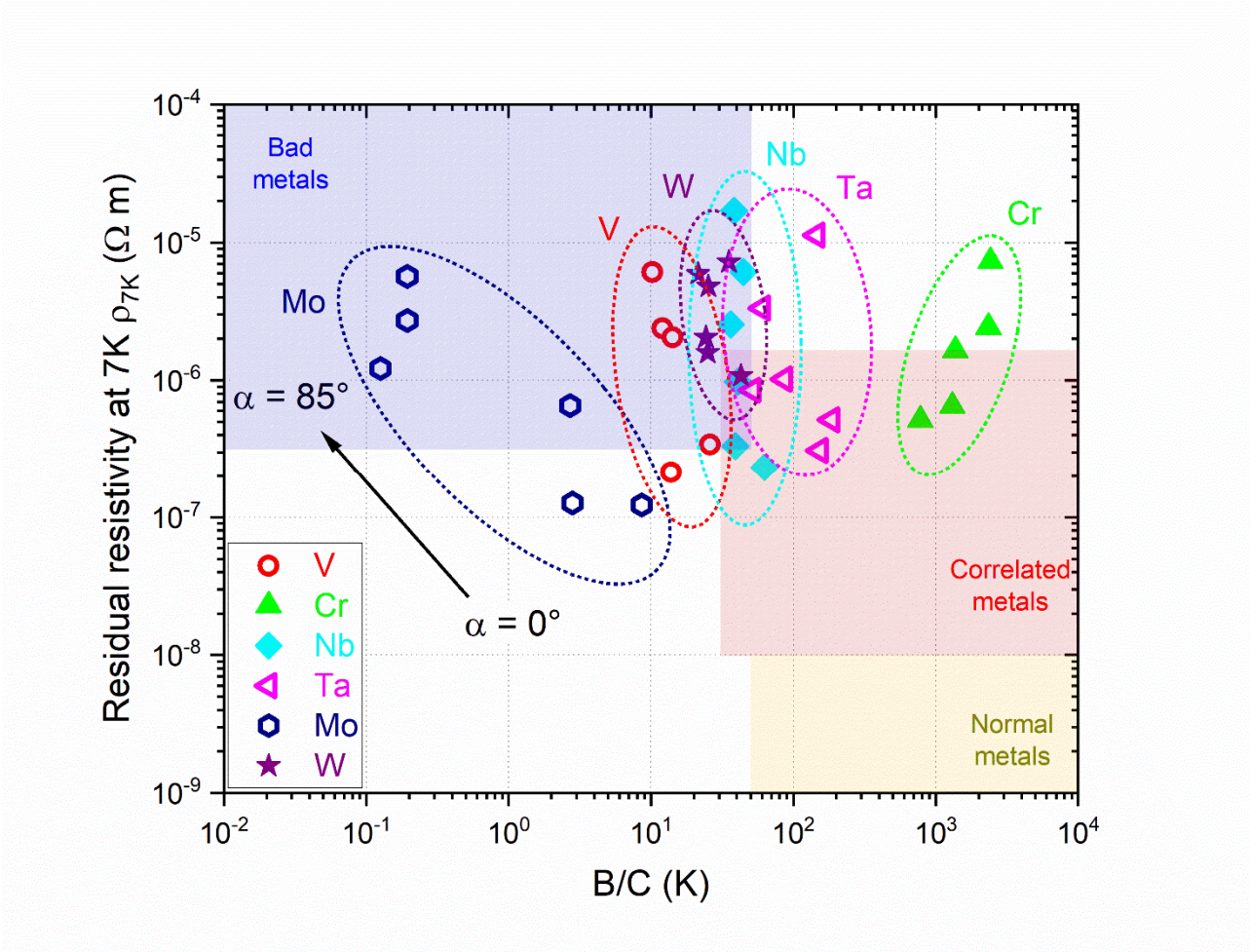

Figure 8: Classification of the six bcc OAD metallic thin films (according to Guo et al. [46]) based on residual resistivity taken at 7 K and B/C coefficient ratio (B and C are determined from fitting of ρ vs. T from Eq. (6)). Nature of the deposited metal and deposition angle α both influence the classification of OAD thin films.

Concerning the B/C ratio, the ρ *vs.* T behavior of these six bcc OAD thin films is clearly determined by the relative importance of B and C coefficients. Excluding OAD Cr thin films (cf. § 4.3 for discussion in detail), even conventional thin films (α = 0°) show a wide range of B/C ratios regarding the nature of the metal. B/C is lower than 10^1 for Mo films, whereas Ta films exhibit the highest ratio, exceeding 10^2. For such conventional deposition conditions (α = 0°), these metallic thin films cannot be assumed as bad metals, but rather as correlated metals (in the limit of normal metals although boundaries between each zone is not clearly defined [38]). One can notice that improving purity and crystalline structure of the films would reduce their residual resistivity and they would

become normal metals. Increasing the deposition angle from 0° to 85° shifts the OAD thin films to the bad metals zone. For each metal, the B/C coefficient tends to be reduced with the strongest change for Mo films. This again verifies the saturation effect in Mo films arising at higher temperature compared to other metallic films, and thus a delayed electron-phonon scattering. OAD Cr thin films exhibit a surprising and opposite effect. This means that Hussey formalism applied to Cr (*i.e.*, T-linear with B coefficient and T-quadratic with C coefficient components and in parallel with a saturation term) does not properly describe the ρ *vs.* T behavior for various deposition angles.

4.3. Cr films: A more complex system

Instead of tending to a constant residual resistivity at the lowest temperatures, one can notice an upturn in resistivity below a few tens of Kelvin. This is typically observed for some metallic alloys containing dilute magnetic constituents giving rise to the Kondo effect [70], or when the film thickness reduces down to a few nanometers [52]. For other metallic systems free of any magnetic constituent but conducive to structural disorder, this resistivity minimum is often assigned to electron-electron interactions [71]. Therefore, the shunt resistor model successfully applied for the five bcc OAD thin films (§ 4.2), or the classical Bloch-Grüneisen model able to reproduce the low-temperature resistivity evolution of Ti, Zr and Hf OAD thin films (§ 4.1), does not match for Cr ones and for the full range of temperatures (Fig. 9). A systematic saturation effect of resistivity is measured as the temperature rises with a minimum at temperatures close to 50 K. In addition, a maximum of resistivity is recorded for Cr thin films obliquely deposited with $\alpha = 85°$, which supports the observation that ρ *vs.* T of OAD Cr thin films exhibit a complex behavior. An electron-electron scattering phenomenon can be suggested involving a $T^{1/2}$ temperature dependence of resistivity at low temperatures [51, 78]. More recently, Li *et al.* [73] also showed a resistivity minimum around 90 K in Be films. The authors showed that electron-phonon-impurity interference effect mainly contributes to the ρ *vs.* T compared to the electron-electron interaction because of the high Debye temperature θ_{Be} of beryllium (θ_{Be} = 1481 K for bulk Be at 0 K). In the case of Cr bulk, θ_{Cr} = 606 K at 0 K and thus electron-phonon-impurity

interference can be neglected. On the other hand, Boekelheide *et al.* [43] interestingly reported resistivity *vs.* temperature from 0.6 to 300 K for epitaxial and polycrystalline Cr thin films. They measured a resistivity minimum in the temperature range of 50 K with a magnitude depending on the sputtering pressure implemented for the film deposition, and as a function of a post- deposition annealing temperature. They successfully fitted the ρ *vs.* T data to a model including the electron-phonon scattering and resonant impurity scattering for temperatures in-between 2-150 K using the following equation:

$$\rho(T) = \rho_0 + \frac{\rho_0^{res}}{1+\left(\frac{T}{\theta^{res}}\right)^2} + D \times \left(\frac{T^5}{\theta^6}\right) \times \int_0^{\frac{\theta}{T}} \frac{x^5}{(e^x-1)\,(1-e^{-x})}\,dx \qquad (8)$$

where ρ_0 is the residual resistivity (Ω m), ρ_0^{res} the magnitude of resonant resistivity (Ω m), θ^{res} a resonant scattering energy parameter (Ω m K^{-1}), D a constant (Ω m K) and θ the Debye temperature (K).

Since ρ *vs.* T of OAD Cr thin films show very similar behaviors in the low range of temperatures, we applied a least-squares fit of equation (8) to our resistivity data recorded from 7 to 150 K. For the upper temperature range (*i.e.*, 150 to 300 K), we applied the former fitting procedure involving equation (6) for bcc metals because Cr films exhibit a significant saturation effect of resistivity when the temperature is higher than 150 K (cf. sections VI and VII of Supplementary Materials). Results presented in Fig. 9 show the very good agreement between experimental data (Exp. with black and blue open circles) and fits (Th. with red and green solid lines) for the two temperature ranges (7-150 K and 150-300 K, respectively). The fitted parameters obtained with home-made Python programs (cf. Supplementary Materials) for all deposition angles, and for the temperature ranges 7-150 K and 150-300 K are tabulated in Tables 1 and 2, respectively.

For all OAD Cr thin films, ρ *vs.* T show a saturation effect of resistivity with the addition of a maximum $\rho = 1.46\times10^{-5}$ Ω m at around 260 K for Cr films prepared with a deposition angle of 85°. As earlier noticed for the other hcp and bcc metallic films and as typically reported many metallic compounds [23-26, 29, 30], resistivity is largely enhanced as the deposition angle becomes grazing with a change of nearly two orders of magnitude between Cr films prepared with α = 0 and 85°. Again,

the growing voided architecture *vs.* α combined with the rising number of structural defects and impurities all contribute to reduce the electron mean free path, and consequently emphasize the resistive character of OAD Cr thin films.

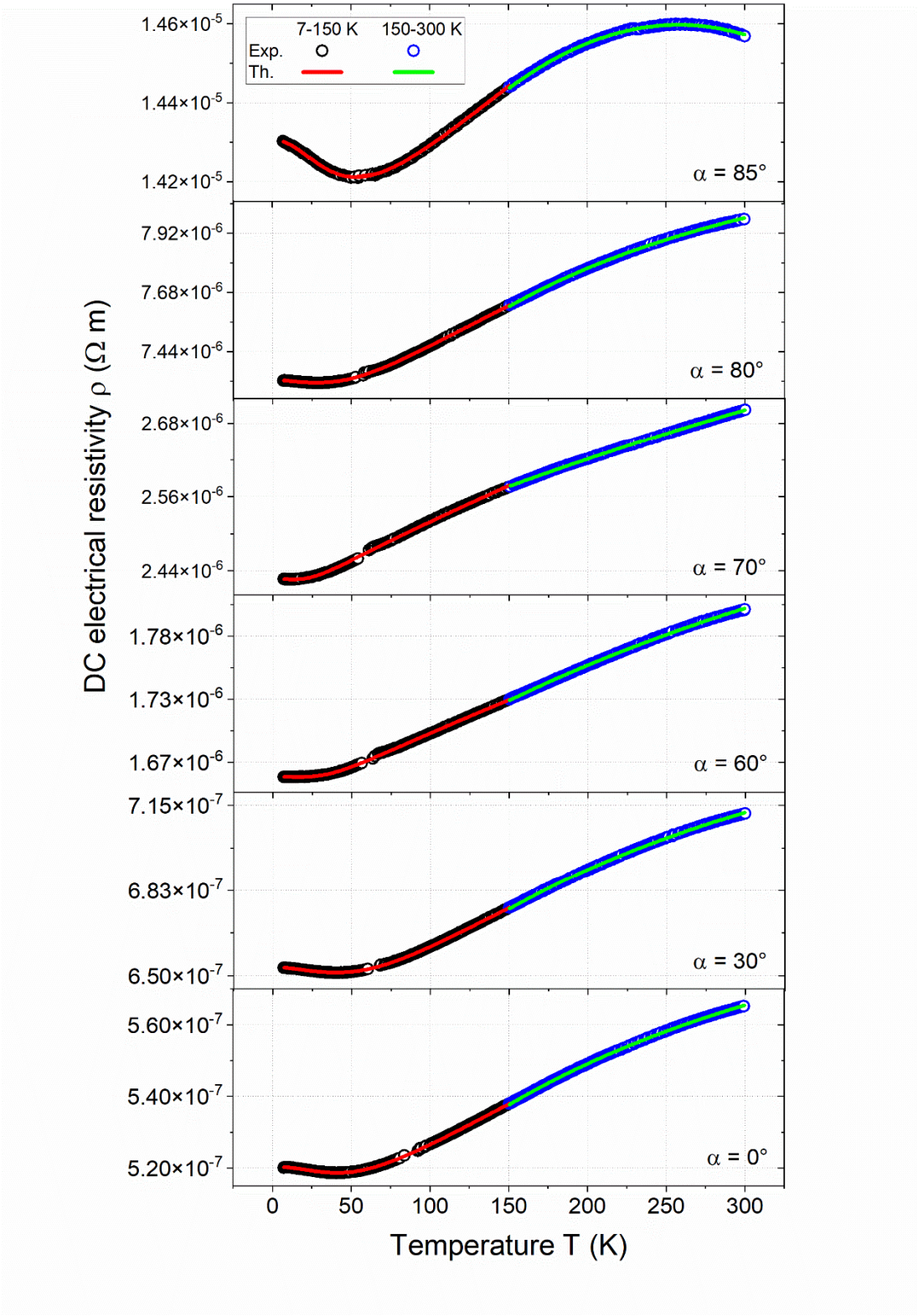

Figure 9: DC electrical resistivity ρ as a function of the temperature T for Cr films sputter-deposited with a systematic increase of the deposition angle α from 0 to 85°. Open circles correspond to

experimental data (Exp.), whereas lines represent fitting (Th.) from Eq. (8) for temperatures in-between 7-150 K (red line) and from Eq. (6) for temperatures in-between 150-300 K (green line).

Table 1: Fitted parameters vs. deposition angle α obtained for Cr thin films from ρ vs. T measurements and assuming Eq. (8) for the temperature range 7-150 K. ρ_0^{res} is the magnitude of resonant resistivity (Ω m), θ^{res} a resonant scattering energy parameter (Ω m K^{-1}), D a constant (Ω m K), θ the Debye temperature (K), ρ_0 the residual resistivity (Ω m). $D/4\theta^2$ is the resulting linear resistivity slope at high temperature (Ω m K^{-1}). Fitting accuracy of the data is below 1%.

α (°)	0	30	60	70	80	85
ρ_0^{res} (Ω m)	1.04×10^{-8}	4.30×10^{-9}	2.44×10^{-9}	3.25×10^{-9}	1.98×10^{-8}	2.07×10^{-7}
θ^{res} (Ω m K^{-1})	68.6	33.9	38.3	12.8	17.0	44.0
D (Ω m K)	8.92×10^{-5}	1.76×10^{-4}	1.07×10^{-4}	1.10×10^{-4}	1.30×10^{-3}	1.35×10^{-3}
θ (K)	318	409	222	157	341	343
ρ_0 (Ω m)	5.10×10^{-7}	6.49×10^{-7}	1.65×10^{-6}	2.42×10^{-6}	7.31×10^{-6}	1.41×10^{-5}
$D/4\theta^2$ (Ω m K^{-1})	2.21×10^{-10}	2.63×10^{-10}	5.43×10^{-10}	1.12×10^{-9}	2.79×10^{-9}	2.87×10^{-9}

Table 2: Fitted parameters vs. deposition angle α obtained for Cr thin films from ρ vs. T measurements and assuming Eq. (6) for the temperature range 150-300 K. Fitting accuracy of the data is below 1%.

α (°)	0	30	60	70	80	85
ρ_0 (Ω m)	4.77×10^{-7}	5.95×10^{-7}	1.59×10^{-6}	2.42×10^{-6}	6.50×10^{-6}	1.37×10^{-5}
ρ_{Sat} (Ω m)	4.77×10^{-7}	4.77×10^{-7}	2.42×10^{-6}	2.42×10^{-6}	2.42×10^{-6}	-3.68×10^{-4}
B (Ω m K^{-1})	6.12×10^{-10}	8.32×10^{-10}	1.15×10^{-9}	1.20×10^{-9}	1.54×10^{-8}	7.11×10^{-9}
C (Ω m K^{-2})	7.85×10^{-13}	6.36×10^{-13}	8.39×10^{-13}	5.12×10^{-13}	6.35×10^{-12}	-1.38×10^{-11}

The resistivity minimum assigned to resonant scattering from defects in the films evidences deviations from the Matthiessen's rule [43]. The latter should be illustrated with parallel ρ *vs.* T curves for the same material when the amount of defects varies. Results in Fig. 9 are clearly inconsistent with this rule with a growing slope in the linear part taken at 150 K, and a resistivity minimum depending on the deposition angle. In order to better understand how α influences the electronic transport in the low temperature range, fitted parameters reported in Table 1 have to be considered. At first, the Bloch-Grüneisen prefactor defined by $D/4\theta^2$, represents the slope of the Bloch-Grüneisen function where the resistivity is linear in temperature, *i.e.*, around 150 K for our films. This prefactor is equal to $(d\rho/dT)_{150K}$ that is directly related to the electron-phonon coupling constant, namely λ_{tr}. Data from Table 1 show that $D/4\theta^2$ and ρ_0 are proportional (despite a small discrepancy for $\alpha = 85°$). This evolution reveals that electronic transport properties of OAD Cr thin films are mainly influenced by geometric constrictions [51]. This means that electrons move with longer and tortuous paths through the film, corresponding to an increased effective length of the sample.

It is also interesting remarking that the Debye temperature θ obtained from the fitting procedure is systematically lower than the bulk one (θ_{Bulk} = 606 K at 0 K) whatever the deposition angle, and as previously discussed for hcp metallic films in § 4.1. This is explained by the phonon softening phenomenon (variation of the phonon density of states decreasing the phonon energy), which is favored as disorder in the films increases and corresponds to a rising deposition angle. This result agrees well with the evolution of the derivative of resistivity at 100 K $(d\rho/dT)_{100K}$ commonly used as an indicator of the electron-phonon coupling constant, and also reduced in other OAD metallic thin films prepared with the highest deposition angles [30].

The two fitting parameters ρ_0^{res} and θ^{res} related to the resonant impurity scattering both characterize the resistivity minimum with ρ_0^{res} corresponding to the magnitude of the minimum, and θ^{res} a resonant scattering energy parameter. Assuming a simple linear relationship between ρ_0^{res} and ρ_0 indicates that resonant scattering mainly contributes to the increase of ρ_0 as deposition angle tends to grazing values [43]. Although these two parameters actually increase as a function of α (Table 1), their

proportionality is not obvious, which means that the resonant impurity scattering phenomenon is not the only mechanism explaining the evolution of the residual resistivity. On the same line, θ^{res} is not a constant as α changes but rather reduces. This suggests that there are different types of localized states produced by the defects. Since OAD process favors the development of a porous architecture *vs.* α, structural defects due to the OAD growth are not the only scattering source, *i.e.*, all free electrons do not participate in the same way in the resonance scattering, but other factors due to voids between and inside the columnar structure (*e.g.*, oxygen as dopant, impurities among others) have to be considered.

Regarding the fitted parameters obtained in the temperature range 150-300 K (Table 2), their variations with α have been discussed previously in § 4.2 and compared to other bcc metals in Fig. 5 to 8. For Cr films prepared with α = 85°, it should however be noticed that negative values of ρ_{Sat} and C fitted parameters have been required to get a good agreement between experiment and equation (6). These negative figures are currently meaningless. They require further investigations and obviously remain an open question.

The resistivity maximum recorded for Cr films prepared with α = 85° (and well fitted with Eq. (6)) gives rise to an unexpected behavior since this kind of maximum is sometimes observed for other metallic alloys [44-46] but to the best of our knowledge, never for single metallic films. For binary, ternary or even multinary compounds, the development of such a resistivity maximum always depends on the composition. For our OAD Cr thin films, despite the occurrence of oxygen in the films around a few at. % (no clear trend of the oxygen content *vs.* α), films are mainly made of Cr metal. As a result, some competing free electron scattering mechanisms due to impurities, growing and structural defects, and voids through and inside the columnar structure have to be regarded. As stated before in § 3, Krasny *et al.* [47] explained extrema in the ρ *vs.* T. evolution by an additional scattering of electrons on rotons. In other words, anomalous features of the electron-phonon dispersion curves of metals also affect the electronic transport properties and so their resistivity temperature dependence. Some metals can show some minima in their dispersion curves, namely roton-like dips. These interactions act as additional scattering for free electrons leading to abnormal resistivity changes as temperature increases (resistivity

upturn). Roton-like phenomena correspond to nests on the Fermi surface. They are usually connected to the bad metal behavior and thus make some significant deviations from the Bloch-Grüneisen law. For transition metals, a maximum of resistivity as a function of the temperature is not expected but only a smooth increase with a saturation effect in some instances (like for OAD bcc films other than Cr). However, dips in the phonon dispersion associated with Fermi surface nesting is a Kohn anomaly, which may happen in alloys and other compounds. In elemental metals and especially in transition metals, such a characteristic is unusual, except in Cr (and less in Mo) due to a well-nested Fermi surface assigned to a half-filled 3d-band [74]. As a result, these nesting conditions strengthen the electron-phonon coupling and favor roton-like excitations.

5. Conclusions

The purpose of this study was to understand the electronic transport properties in the low temperature range of early transition metal (groups 4, 5 and 6) thin films sputter-deposited by oblique angle deposition. To this end, nine metals: Ti, V, Cr, Zr, Nb, Mo, Hf, Ta, and W, were prepared with deposition angle α increasingly changing from 0 to 85° and with the same film thickness of 400 nm. DC electrical resistivity *vs.* temperature measurements were performed from 7 to 300 K. Increasing the deposition angle from 0° to the highest grazing value produces a more voided medium and a rising number of structural defects. The resistivity development was mainly attributed to the enhancement of the electron scattering by surfaces and grain boundaries induced by a much more porous film's architecture.

For the three hcp metallic thin films (Ti, Zr and Hf), the classical Bloch-Grüneisen law accurately describes the conductivity mechanism whatever the deposition angle. An independent temperature contribution is obtained as the temperature tends to 0 K that corresponds to electron-defect (or impurity) interactions and represents the residual resistivity. It is associated with a linear temperature dependence of the resistivity as the temperature rises. The latter is related to electron-phonon interactions, as typically observed for bulk metals and alloys.

A two-channel scattering description of resistivity (Hussey formalism) was successfully applied to OAD bcc metallic thin films made of V, Cr, Nb, Mo, Ta and W elements. It consists of a temperature-linear and quadratic component added to the residual resistivity and in parallel with a saturation term, thus providing a good description of the resistivity *vs.* temperature and for various deposition angles. A saturation effect (depending on the nature of the metal and deposition angle) of resistivity was observed as the temperature rises. These six systems were classified as a function of fitted parameters connected to the residual and saturation resistivities. It was shown that correlated metals (close to normal metals) were produced by conventional sputtering. Using a higher deposition angle shifts the thin film characteristics from correlated to bad metals due to the growing number of voids, defects and impurities in the tilted columnar architecture. However, Mo films exhibited a slight saturation effect at higher temperature compared to other metallic films, meaning a delayed electron-phonon scattering.

OAD Cr thin films showed a surprising resistivity *vs.* temperature behavior depositing with a more grazing deposition angle. The Hussey formalism applied to Cr with T-linear and T-quadratic components and in parallel with a saturation term does not properly describe the complete ρ *vs.* T behavior. It was used for temperatures higher than 150 K where electronic transport properties of Cr films were governed by geometric constrictions. For the lowest temperatures (from 7 to 150 K), anomalous features of the electron-phonon dispersion curves (additional scattering of electrons on rotons) were assumed to describe the resistivity minimum.

Combining experimental resistivity *vs.* temperature data and theoretical analyses based on various electron scattering mechanisms, our study provides fundamental insights for understanding electrical properties OAD metallic thin films prepared by sputtering, particularly at low temperatures. Other transition metals with more filled d-bands and adopting other crystallographic structures or more innovative architectures such as core-shell or Janus-like structures, could further extend these investigations. These original systems would require further investigations (e.g., annealing treatments to change the defect concentration) to better understand electron scattering mechanisms. They also lead to an array of applications focused on sensing, cryogenic and involving physical phenomena at the micro- and nanoscales.

CRediT authorship contribution statement

Nicolas Martin: Writing - review & editing; Software; Supervision; Funding acquisition. **Hamidreza Gerami:** Data curation; Validation; Writing - review & editing. **Antonio J. Santos:** Validation; Writing - review & editing. **Francesco M. Morales:** Validation; Writing - review & editing. **Fabien Amiot:** Validation; Writing - review & editing. **Jean-Marc Cote:** Data curation; Validation; Writing - review & editing. **Joseph Gavoille:** Validation; Writing - review & editing. **Jean-Baptiste Sanchez:** Validation; Writing - review & editing. **Aurélien Besnard:** Validation; Writing - review & editing.

All authors have read and agreed to the published version of the manuscript.

Declaration of Competing Interest

The authors declare that they have no known competing financial interests or personal relationships that could have appeared to influence the work reported in this paper.

Data availability

Data will be made available on request.

Acknowledgements

The authors thank Eliot Martin from Université Paris Cité (France) for assistance in developing and optimizing Python programs. This work has been achieved in the frame of the EIPHI Graduate school (contract "ANR-17-EURE-0002" and by the Bourgogne-Franche-Comté Region. It has also been partly supported by the French RENATECH network and its FEMTO-ST technological facility.

Appendix A: Supplementary Materials

Supplementary Materials to this article can be found on line at https:// …

References

[1] M. Nur-E-Alam, B.K. Yap, M.K. Basher, M.A. Islam, M.K. Hossain, M.E.M. Soudagar, N. Das, M. Vasiliev, T.S. Kiong, Multifunction prospects of physical vapor-deposited silver-based metal-dielectric nanocomposites films, J. Sci., 10 (2025) 100871-16. https://doi.org/10.3390/app11156746

[2] M.R. Islam, P. Karna, N. Bhatt, S. Thakur, H. Heinrich, D.M. Hirt, S. Zare, C. Jezewski, R.T.P. Lee, K. Tapily, J.T. Gaskins, C.D. Landon, S.W. King, A. Giri, P.E. Hopkins, Unveiling phonon contributions to thermal conductivity and the applicability of the Wiedemann-Franz Law in Ruthenium and Tungsten thin films, Adv. Funct. Mater., 36 (2026) e11592-13. https://doi.org/10.1002/adfm.202511592

[3] A. Zaccone, Thickness-dependent conductivity of nanometric semiconductor thin films, Phys. Rev. B, 9 (2025) 046001-5. https://doi.org/10.1103/physrevmaterials.9.046001

[4] S. Tangui, S. Hurand, R. Aljasmi, A. Benmoumen, M.L. David, P. Moreau, S. Morisset, S. Célérier, V. Mauchamp, 2D versus 3D-like electrical behavior of MXene thin films: Insights from weak localization in the role of thickness, interflake coupling and defects, Small, 21(1) (2025) 2406334-12. https://doi.org/10.1002/smll.202406334

[5] A. Casu, A. Chiodoni, Y.P. Ivanov, G. Divitini, P. Milani, A. Falqui, *In Situ* TEM investigation of thermally induced modifications of cluster-assembled Gold films undergoing resistive switching: Implications for nanostructured neuromorphic devices, ACS Appl. Nano Mater., 7 (2024) 7203-7212. https://doi.org/10.1021/acsanm.3c06261

[6] H. LaBollita, J. Lee-Hand, F.B. Kugler, L. Van Muñoz, S. Beck, A. Hampel, J. Kaye, A. Georges, C.E. Dreyer, Low-temperature transport in high-conductivity correlated metals: A density-functional plus dynamical mean-field study of cubic perovskites, Phys. Rev. B, 113 (2026) 085125-16. https://doi.org/10.1103/71c6-sb7v

[7] J.P. Soulié, K. Sankaran, B. Van Troeye, A. Leśniewska, O.V. Pedreira, H. Oprins, G. Delie, C. Fleischmann, L. Boakes, C. Rolin, L.A. Ragnarsson, K. Croes, S. Park, J. Swerts, G. Pourtois, Z. Tőkei, C. Adelmann, Selecting alternative metals for advanced interconnects, J. Appl. Phys., 136 (2024) 171101-35. https://doi.org/10.1063/5.0224027

[8] S. Kumbhakar, T.K. Maji, B. Tongbram, S. Mandal, S.H. Soundararaj, B. Debnath, P. Sai T, M. Jain, H.R. Krishnamurty, A. Pandey, A. Ghosh, Engineering ultra-strong electron-phonon coupling and nonclassical electron transport in crystalline gold with nanoscale interfaces, Nature Commun., 16 (2025) 61-9. https://doi.org/10.1038/s41467-024-55435-z

[9] F. Corbella, V. Haspot, Y. Zheng, L. Largeau, D. Guimard, H. Montigaud, R. Lazzari, An application of the Mayadas-Shatzkes model of thin film resistivity to Ag-based thermal control coatings, ACS Appl. Mater. Interfaces, 17(36) (2025) 51431-51447. https://doi.org/10.1021/acsami.5c10481

[10] E. Coleman, A. Kelly, C. Gabbett, L. Doolan, S. Liu, N. Yadav, J.K. Vij, J.N. Coleman, Extracting the temperature dependence of both nanowire resistivity and junction resistance from electrical measurements on printed Silver nanowire networks, ACS Appl. Electron. Mater., 7 (2025) 806-815. https://doi.org/10.1021/acsaelm.4c01965

[11] U. Pinsook, P. Tanthum, Universal resistivity from electron-phonon interaction based on Einstein model: Application to near-room temperature superconductors, Next Materials, 6 (2025) 100302-5. https://doi.org/10.1016/j.nxmate.2024.100302

[12] N.G. Ptitsina, G.M. Chulkova, K.S. Il'in, A.V. Sergeev, F.S. Pochinkov, E.M. Ghershenzon, Electron-phonon interaction in disordered metal films: The resistivity and electron dephasing rate, Phys. Rev. B, 56 (1997) 10089-10096. https://doi.org/10.1103/physrevb.56.10089

[13] W.C. Hsu, C.C. Chen, Y.H. Lin, H.K. Lin, H.T. Chiu, J.J. Lin, Metallic conduction and large electron-phonon-impurity interference effect in single TiSi nanowires, Nanoscale Res. Lett., 7 (2012) 500-5. https://doi.org/10.1186/1556-276x-7-500

[14] E. Broitman, P. Alonso, R. Zimmerman, Deviations from Matthiessen' s rule in continuous metal films, Thin Solid Films, 277 (1996) 192-195. https://doi.org/10.1016/0040-6090(95)08018-x

[15] A. Verma, K. Bhatt, J.D. Tanwar, J.S. Tawale, P. Kushwaha, P.K. Siwach, H.K. Sinch, Evolution of ferromagnetism and metallicity in RF magnetron sputtered Mn-Ni-Sn Heusler alloy thin films, Results Surf. Interfaces, 20 (2025) 100616-9. https://doi.org/10.2139/ssrn.4948001

[16] S. Li, C. Song, Y. Li, J. Ge, Z. Li, Y. Zheng, L. Li, J. Li, Resistivity-temperature behavior of Cu-Ni-Al alloys strengthened by coherent precipitation within a wide composition range, Vacuum, 240 (2025) 114578-5. https://doi.org/10.1016/j.vacuum.2025.114578

[17] S. Sato, K. Maki, M. Ito, S. Suzuki, Factors affecting the physical properties of electrically conductive copper and dilute copper alloys, Mater. Trans., 64(9) (2023) 2039-2050. https://doi.org/10.2320/matertrans.mt-m2023067

[18] C. Adelman, On the extraction of resistivity and area of nanoscale interconnect lines by temperature-dependent resistance measurements, Solid State Electron., 152 (2019) 72-80, https://doi.org/10.1016/j.sse.2018.12.005. https://doi.org/10.1016/j.sse.2018.12.005

[19] V. Palenskis, E. Zitkevicius, Phonon mediated electron-electron scattering in metals, World Journal of Condensed Matter Physics, 8 (2018) 115-129. https://doi.org/10.4236/wjcmp.2018.83008

[20] V. Palenskis, New insight into electric force in metal and the quadratic electrical resistivity law of metals at low temperatures, Metals, 14 (2024) 526-15. https://doi.org/10.3390/met14050526

[21] E.F. Talantsev, The dominance of non-electron-phonon charge carrier interaction in highly-compressed superhybrides, Supercond. Sci. Tech., 34 (2021) 115001-16. https://doi.org/10.1088/1361-6668/ac19f3

[22] N.G. Ptitsina, G.M. Chulkova, E.M. Gershenzon, M.E. Gershenzon, Influence of the interference of electron-phonon and electron-impurity scattering on the conductivity of unordered Nb films, JETP, 80 (1985) 960-964.

[23] R. El Beainou, J.M. Cote, V. Tissot, V. Potin, N. Martin, Resistivity anisotropy of tilted columnar W and W-Cu thin films, Surf. Coat. Technol., 421 (2021) 127412-11. https://doi.org/10.1016/j.surfcoat.2021.127412

[24] Z. Ali, D. Basaula, W. Zhou, J. Brock, M. Khan, K.F. Eid, Controlling the charge transport mode in permalloy films using oblique angle deposition, J. Magn. Magn. Mater. 484 (2019) 430–436, https://doi.org/10.1016/j.jmmm.2019.03.087.

[25] Z. Ali, D. Basaula, K.F. Eid, M. Khan, Anisotropic properties of oblique angle deposited permalloy thin films, Thin Solid Films 735 (2021) 138899-8, https://doi.org/10.1016/j.tsf.2021.138899.

[26] H. Gerami, G. Vilar Soler, J.M. Cote, J.B. Sanchez, N. Martin, Correlations between structure and electrical properties of Cr–Ta thin films prepared by oblique angle co-sputtering, Surf. Coat. Technol., 503 (2025) 132002-8. https://doi.org/10.1016/j.surfcoat.2025.132002

[27] P. Wissman, H.U. Finzel, Electrical resistivity of thin metal films, Springer-Verlag, Berlin Heidelberg, (2007). https://doi.org/10.1007/3-540-48490-6

[28] A. Siad, A. Besnard, C. Nouveau, P. Jacquet, Critical angle in DC magnetron GLAD thin films, Vacuum, 131 (2016) 305-311. https://doi.org/10.1016/j.vacuum.2016.07.012

[29] A. Besnard, N. Martin, L. Carpentier, B. Gallas, A theoretical model for the electrical properties of chromium thin films sputter deposited at oblique incidence, J. Phys. D: Appl. Phys., 44 (2011) 215301-8. https://doi.org/10.1088/0022-3727/44/21/215301

[30] H. Gerami, J.M. Cote, A.J. Santos, N. Martin, Low temperature dependence of electrical resistivity in obliquely sputter-deposited transition metal thin films, Surf. Interfaces, 54 (2024) 105113-11. https://doi.org/10.1016/j.surfin.2024.105113

[31] M.O. Jensen, M.J. Brett, Porosity engineering in glancing angle deposition thin films, Appl. Phys. A, 80 (2005) 763-768. https://doi.org/10.1007/s00339-004-2878-5

[32] A. Dolatshahi-Pirouz, C.P. Pennisi, S. Skeldal, M. Foss, J. Chevallier, V. Zachar, P. Andreasen, K. Yoshida, F. Besenbacher, The influence of glancing angle deposited nano-rough platinium surfaces on the adsorption of fibrinogen and the proliferation of primary human fibroblasts, Nanotechnology, 20 (2009) 095101-9. https://doi.org/10.1088/0957-4484/20/9/095101

[33] S. Mahieu, G. Buyle, P. Ghekiere, S. Heirwegh, R. De Gryse, D. Depla, Mechanism of biaxial alignment in thin films deposited by magnetron sputtering, Thin Solid Films, 515 (2006) 416-420. https://doi.org/10.1016/j.tsf.2005.12.226

[34] C.R. Tellier, Effect of defect structure on the electrical conduction mechanism in metallic thin films, J. Mater. Sci., 20 (1985) 1901-1919. https://doi.org/10.1016/0040-6090(84)90407-3

[35] G. Verite, F. Villaime, C.C. Fu, Anisotropy of the vacancy migration in Ti, Zr and Hf hexagonal close-packed metals from first principles, Solid State Phenom., 129 (2007) 75-81. https://doi.org/10.4028/www.scientific.net/ssp.129.75

[36] A. Bid, A. Bora, A.K. Raychaudhury, Temperature dependence of the resistance of metallic nanowires of diameter ≥ 15 nm: Applicability of Bloch-Grüneisen theorem, Phys. Rev. B, 74 (2006) 035426-9, https://doi.org/10.1103/physrevb.74.035426.

[37] D.R. Lide (Ed.), CRC Handbook of Chemistry and Physics, Internet Version, 2005, CRC Press, Boca Raton, FL, 2005 (<http://www.hbcpnetbase.com>). https://doi.org/10.1021/ja041017a

[38] Q. Guo, C. Magen, M.J. Rozenberg, B. Noheda, Phenomenological classification of metals based on resistivity, Phys. Rev. B 106 (2022) 085141–085146, https://doi.org/10.1103/physrevb.106.085141.

[39] Y.P. Timalsina, A. Horning, R.F. Spivey, K.M. Lewis, T.S. Kuan, G.C. Wang, T.M. Lu, Effects of nanoscale surface roughness on the resistivity of ultrathin epitaxial copper films, Nanotechnology, 26 (2015) 075704-10. https://doi.org/10.1088/0957-4484/26/7/075704

[40] A. Sergeev, V. Mitin, Electron-phonon interaction in disordered conductors: Static and vibrating scattering potentials, Phys. Rev. B, 61 (2000) 6041-6047. https://doi.org/10.1103/physrevb.61.6041

[41] Z. Cheng, L. Liu, S. Xu, M. Lu, X. Wang, Temperature dependence of electrical and thermal conduction in single silver nanowire, Sci. Rep., 5 (2015) 10718-12. https://doi.org/10.1038/srep10718

[42] Z. Fisk, G.W. Webb, Saturation of the high-temperature normal-state electrical resistivity of superconductors, Phys. Rev. Lett., 36 (1976) 1984-1986. https://doi.org/10.1103/physrevlett.36.1084

[43] Z. Boekelheide, D.W. Cooke, E. Helgren, F. Hellman, Resonant impurity scattering and electron-phonon scattering in the electrical resistivity of Cr films, Phys. Rev. B, 80 (2009) 134426-12. https://doi.org/10.1103/physrevb.80.134426

[44] M.V. Kondrin, V.R. Gizatullin, S.V. Popova, A.G. Lyapin, V.V. Brazhkin, V.Y. Ivanov, A.A. Pronin, Y.B. Lebed, R.A. Sadykov, Electrotransport and magnetic properties of Cr-GaSb phases synthesized under high pressure, J. Phys.: Condens. Matter, 23 (2011) 446001-7. https://doi.org/10.1088/0953-8984/23/44/446001

[45] N.R. Poniatowski, T. Sarkar, S. Das Sarma, R.L. Greene, Resistivity saturation in electron-doped cuprate, Phys. Rev. B, 103 (2021) L020501-5. https://doi.org/10.1103/physrevb.103.l020501

[46] D. Shaltiel, M. Reshotko, A. Grayevsky, J.P. Burgert, J.N. Daou, P. Vajda, Saturation with temperature of the electrical resistivity and CESR line width in $TiBe_2$, J. Phys. F.: Met. Phys., 18 (1988) 2445-2450. https://doi.org/10.1088/0305-4608/18/11/016

[47] Y.P. Krasny, J. Krawczyk, N.P. Kovalenko, V.T. Shvets, Electrical resistivity of amorphous simple metals at moderately low temperatures, Physica B, 269 (1999) 221-226. https://doi.org/10.1016/s0921-4526(99)00149-0

[48] D.G. Westlake, L.C.R. Alfred, Determination of the Debye characteristic temperature of vanadium from the Bloch-Grüneisen relation, J. Phys. Chem. Solids, 29 (1968) 1931-1934. https://doi.org/10.1016/0022-3697(68)90043-7

[49] G.T. Meaden, Electrical resistance of metals, Springer Science, New York, (1965). https://doi.org/10.1007/978-1-4899-5717-7

[50] O.L. Anderson, A simplified method for calculating the Debye temperature from elastic constants, J. Phys. Chem. Solids, 24 (1963) 909-917. https://doi.org/10.1016/0022-3697(63)90067-2

[51] J. Joseph, C. Bansal, K.J. Reddy, A. Rajanikanth, Electron-electron interaction dominated resistivity minimum in quasi-continuous Ag nanocluster films, AIP Adv., 10 (2020) 125223-4. https://doi.org/10.1063/5.0033098

[52] A. Jayakumar, V. Dixit, S. Jose, V.B. Kamble, D. Jaiswal-Nagar, Charge transport variation from Bloch-Grüneisen to Mott variable range hopping and transport change due to hydrogenation in palladium thin films, Sci. Rep., 11 (2021) 22298-18. https://doi.org/10.1038/s41598-021-01787-1

[53] W. Ma, X. Zhang, K. Takahashi, Electrical properties and reduced Debye temperature of polycrystalline thin gold films, J. Phys. D: Appl. Phys., 43 (2010) 465301-8. https://doi.org/10.1088/0022-3727/43/46/465301

[54] N. Martin, E. Martin, J.M. Cote, F. Sthal, J. Gavoille, M. Raschetti, S. Oliveri, Low temperature dependence of resistivity in obliquely sputter-deposited gold thin films, Surf. Coat. Technol., 499 (2025) 131884-8. https://doi.org/10.1016/j.surfcoat.2025.131884

[55] Q. Chen, B. Sundman, Calculation of Debye temperature for crystalline structures – A case study on Ti, Zr and Hf, Acta Mater., 49 (2001) 947-961. https://doi.org/10.1016/s1359-6454(01)00002-7

[56] A. Chargui, R. El Beainou, A. Mosset, S. Euphrasie, V. Potin, P. Vairac, N. Martin, Influence of thickness and sputtering pressure on electrical resistivity and elastic wave propagation in oriented columnar tungsten thin films, Nanomaterials, 10(1) 81 (2020) 1-18. https://doi.org/10.3390/nano10010081

[57] R. El Beainou, A. Chargui, P. Pedrosa, A. Mosset, S. Euphrasie, P. Vairac, N. Martin, Electrical conductivity and elastic wave propagation anisotropy in glancing angle deposited tungsten and gold films, Appl. Surf. Sci., 475 (2019) 606-614. https://doi.org/10.1016/j.apsusc.2019.01.041

[58] S.S. Yeh, J.J. Lin, J. Xiunian, Z. Dianlin, Electron-phonon-impurity interference effect in disordered $Au_{56}Pd_{44}$ and IrO_2 thick films, Phys. Rev. B, 72 (2005) 024204-5. https://doi.org/10.1103/physrevb.72.024204

[59] P.B. Allen, Metals with small electron mean-free path: Saturation versus escalation of resistivity, Physica B, 318 (2002) 24-27. https://doi.org/10.1016/s0921-4526(02)00769-x

[60] H. Wiesmann, M. Gurvitch, H. Lutz, A. Ghosh, B. Schwarz, M. Strongin, P.B. Allen, J.W. Halley, Simple model for characterizing the electrical resistivity in A-15 superconductors, Phys. Rev. Lett., 38 (1977) 782-785. https://doi.org/10.1103/physrevlett.38.782

[61] O. Gunnarsson, M. Calandra, J.E. Han, Colloquium: Saturation of electrical resistivity, Rev. Mod. Phys., 75 (2003) 1085-1099. https://doi.org/10.1103/revmodphys.75.1085

[62] J.K. Glasbrenner, B.S. Pujari, K.D. Belashchenko, Deviations from Matthiessen's rule and resistivity saturation effects in Gd and Fe from first principles, Phys. Rev. B, 89 (2008) 174408-10. https://doi.org/10.1103/physrevb.89.174408

[63] N.E. Hussey, K. Takenaka, H. Takagi, Universality of the Mott-Ioffe-Regel limit in metals, Philos. Mag. A-Phys. Condens. Matter Struct. Defect Mech. Prop., 84 (2004) 2847-2864. https://doi.org/10.1080/14786430410001716944

[64] B. Sundqvist, V.K. Tolpygo, Saturation and pressure effects on the resistivity of titanium and two Ti-Al alloys, J. Phys. Chem. Solids, 122 (2018) 41-50. https://doi.org/10.1016/j.jpcs.2018.05.046

[65] B. Sundqvist, Resistivity saturation in crystalline metals: Semi-classical theory versus experiment, J. Phys. Chem. Solids, 165 (2022) 110686-9. https://doi.org/10.1016/j.jpcs.2022.110686

[66] S. Shiri, A. Odeshi, N. Chen, R. Feng, R. Sutarto, Q. Yang, Fcc tantalum thin films deposited by magnetron sputtering, Surf. Coat. Technol., 358 (2019) 942-946. https://doi.org/10.1016/j.surfcoat.2018.12.015

[67] G.B. Rodrigues, N. Martin, F. Amiot, G. Colas, Friction anisotropy dependence on morphology of GLAD W films, Tribol. Int., 206 (2025) 110556-12. https://doi.org/10.1016/j.triboint.2025.110556

[68] T. Hao, Resistivity of various metals described in a wide temperature range with a universal theoretical equation, Physica B, 655 (2023) 414770-6. https://doi.org/10.1016/j.physb.2023.414770

[69] F.G. Cougnon, I.C. Schramm, D. Depla, On the electrical properties of sputter deposited thin films: The role of energy and impurity flux, Thin Solid films, 690 (2019) 137540-7. https://doi.org/10.1016/j.tsf.2019.137540

[70] J. Kondo, Resistance minimum in dilute magnetic alloys, Prog. Theor. Phys. 32 (1964) 37-49. https://doi.org/10.1143/ptp.32.37

[71] S. Banerjee, A.K. Raychaudhuri, Resistivity minima and electron-electron interaction in crystalline alloys of transition metals [$Fe_xNi_{80-x}Cr_{20}$, $63 \geq x \geq 50$], Solid State Commun., 83 (1992) 1047-1051. https://doi.org/10.1016/0038-1098(92)90538-k

[72] Q.F. Zhang, X.Z. Wang, L.S. Wang, H.F. Zheng, L. Lin, J. Xie, X. Liu, Y.L. Qiu, Y.Z. Chen, D.L. Peng, Size-dependent electrical transport properties in Co nanocluster-assembled granular films, Sci. Rep. 7 (2017) 11666-9. https://doi.org/10.1038/s41598-017-11983-7

[73] Z. Li, Y. He, L. Jin, X. Li, B. Luo, Y. Zeng, M. Zhou, J. Zhang, Resistivity minimum in beryllium films, Phys. Status Solidi B-Basic Solid State Phys., 259 (2022) 2100335-7. https://doi.org/10.1002/pssb.202100335

[74] D.G. Laurent, J. Callaway, J.M. Fry, N.E. Brener, Band structure, Fermi surface, Compton profile, and optical conductivity of paramagnetic chromium, Phys. Rev. B, 23 (1981) 4977-4987. https://doi.org/10.1103/physrevb.23.4977

Figure captions

Figure 1: DC electrical resistivity ρ as a function of the temperature T and for different deposition angles α changing from 0° to 85° of: a) Titanium; b) Zirconium and c) Hafnium 400 nm thick films sputter-deposited on glass substrates. A typical metallic-like behavior is measured for these hcp metallic films with a residual resistivity at very low temperature (T less than around 10 K) exhibiting a nearly temperature-independent evolution, whereas a linear temperature-dependence appears when temperature increases and tends to the room temperature.

Figure 2: Derivative of resistivity by temperature at 100 K $(d\rho/dT)_{100K}$ *vs.* DC electrical resistivity at 7 K ρ_{7K} for the three hcp (Ti, Zr, Hf) and the six bcc (V, Cr, Nb, Mo, Ta, W) metallic thin films. Bulk data from [45] can be compared to the film values obtained for conventional sputtering (α = 0°) and the highest deposition angle (α = 85°). The Mott-Ioffe-Regel (MIR) limit is also specified (red dashed line).

Figure 3: Relative resistivity $(\rho - \rho_{7K})/\rho_{300K}$ *vs.* temperature T of: a) Titanium (hcp structure); b) Vanadium (bcc structure) and c) Chromium (bcc structure) thin films prepared with two extreme deposition angles α = 0° and 85°. As the temperature rises, a typical linear temperature-dependence is obtained for Ti films, whereas a saturation effect is measured for vanadium films. Chromium films show a minimum value at low temperature and those obtained with a deposition angle α = 85° give rise to an unusual maximum relative intensity at a temperature T = 262 K.

Figure 4: Fitted parameters, namely a) Debye temperature θ and b) A coefficient, determined from the Bloch-Grüneisen law (Eq. (1) and (2)) as a function of the deposited angle α for the three-hcp metallic thin films: Ti, Zr and Hf.

Figure 5: Resistivity saturation ρ_{Sat} as a function of the deposition angle α of the six bcc metallic thin films: V, Cr, Nb, Mo, Ta and W. The resistivity at saturation ρ_{Sat} is determined from fitting ρ *vs.* T experimental data with equation (6) based on the parallel resistor formalism [68].

Figure 6: Resistivity saturation ρ_{Sat} as a function of the residual resistivity ρ_0 taken at 7K ρ_{7K} (Log scales) of the six bcc metallic thin films: V, Cr, Nb, Mo, Ta and W. Both resistivities similarly increase (more than two orders of magnitude) when the deposition angle α changes from 0° to 85°. ρ_{7K} measured at 7 K is nearly the same as ρ_0 obtained from fitting ρ *vs.* T assuming Eq. (5) (cf. Supplementary Materials). ρ_{Sat} is also determined from the same fitting procedure.

Figure 7: Evolution of a) B and b) C coefficients *vs.* DC electrical resistivity at room temperature ρ_{300K} for the six bcc metallic thin films: V, Cr, Nb, Mo, Ta and W. Both coefficients are determined from the fit of ρ *vs.* T data assuming Eq. (6). The Mott-Ioffe-Regel (MIR) limit is indicated with the red dashed line ($B_{MIT} = 10^{-8}$ Ω m K^{-1}). The effect of the deposition angle α is also shown.

Figure 8: Classification of the six bcc OAD metallic thin films (according to Guo et al. [46]) based on residual resistivity taken at 7 K and B/C coefficient ratio (B and C are determined from fitting of ρ *vs.* T from Eq. (6)). Nature of the deposited metal and deposition angle α both influence the classification of OAD thin films.

Figure 9: DC electrical resistivity ρ as a function of the temperature T for Cr films sputter-deposited with a systematic increase of the deposition angle α from 0 to 85°. Open circles correspond to experimental data (Exp.), whereas lines represent fitting (Th.) from Eq. (8) for temperatures in-between 7-150 K (red line) and from Eq. (6) for temperatures in-between 150-300 K (green line).

Table captions

Table 1: Fitted parameters *vs*. deposition angle α obtained for Cr thin films from ρ *vs*. T measurements and assuming Eq. (8) for the temperature range 7-150 K. ρ_0^{res} is the magnitude of resonant resistivity (Ω m), θ^{res} a resonant scattering energy parameter (Ω m K^{-1}), D a constant (Ω m K), θ the Debye temperature (K), ρ_0 the residual resistivity (Ω m). $D/4\theta^2$ is the resulting linear resistivity slope at high temperature (Ω m K^{-1}). Fitting accuracy of the data is below 1%.

Table 2: Fitted parameters vs. deposition angle α obtained for Cr thin films from ρ vs. T measurements and assuming Eq. (6) for the temperature range 150-300 K. Fitting accuracy of the data is below 1%.